The meiotic LINC complex component KASH5 is an activating adaptor for cytoplasmic dynein

Kirsten E. L. Garner[1]*, Anna Salter[1,2]*, Clinton K. Lau[3], Manickam Gurusaran[4], Cécile Villemant[1], Elizabeth P. Granger[1], Gavin McNee[1], Philip G. Woodman[1], Owen R. Davies[4], Brian E. Burke[2]*, and Victoria J. Allan[1,2]*

*: equal contributions

1: School of Biological Sciences, Faculty of Biology, Medicine and Health, University of Manchester, The Michael Smith Building, Rumford St, Manchester M13 9PT.
2: A*STAR Institute of Medical Biology, 8A Biomedical Grove, #06-06 Immunos, Singapore 138648.
3: MRC Laboratory of Molecular Biology, Francis Crick Avenue, Cambridge Biomedical Campus, Cambridge CB2 0QH, UK
4: Wellcome Centre for Cell Biology, Institute of Cell Biology, University of Edinburgh, Michael Swann Building, Max Born Crescent, Edinburgh EH9 3BF, UK

Present addresses: Brian Burke, A*STAR Skin Research Labs (A*SRL), Biopolis, 8A Biomedical Grove, #06-06 Immunos, Singapore; Elizabeth Granger, University of Central Lancashire, Preston, PR1 2HE, UK; Clinton Lau, Department of Biochemistry, University of Oxford, South Parks Road, Oxford, OX1 3QU, UK; Gavin McNee, University of Birmingham, Edgbaston, Birmingham B15 2TT, UK; Anna Salter, Immunocore Ltd, 92 Park Drive, Milton Park, OX14 4RY, UK; Cécile Villemant, The Automation Partnership, (Cambridge) Limited, York Way, Royston, Hertfordshire, SG8 5WY, UK.

Corresponding author: Viki Allan (viki.allan@manchester.ac.uk), ORCID 0000-0003-4583-0836

A preprint of this manuscript is posted at https://biorxiv.org/cgi/content/short/2022.04.13.488131v1

Abstract

Cytoplasmic dynein-driven movement of chromosomes during prophase I of mammalian meiosis is essential for synapsis and genetic exchange. Dynein connects to chromosome telomeres via KASH5 and SUN1 or SUN2, which together span the nuclear envelope. Here, we show that KASH5 promotes dynein motility in vitro, and cytosolic KASH5 inhibits dynein's interphase functions. KASH5 interacts with either dynein light intermediate chain (DYNC1LI1 or DYNC1LI2) via a conserved helix in the LIC C-terminal, and this region is also needed for dynein's recruitment to other cellular membranes. KASH5's N-terminal EF-hands are essential, as the interaction with dynein is disrupted by mutation of key calcium-binding residues, although it is not regulated by cellular calcium levels. Dynein can be recruited to KASH5 at the nuclear envelope independently of dynactin, while LIS1 is essential for dynactin incorporation into the KASH5-dynein complex. Altogether, we show that the trans-membrane protein KASH5 is an activating adaptor for dynein, and shed light on the hierarchy of assembly of KASH5-dynein-dynactin complexes.

Introduction

To conceive healthy offspring, a paternal sperm and maternal egg must be created, which requires the specialised form of cell division, meiosis, in which maternal and paternal homologues pair in prophase I to allow the swap of genetic material by synapsis, generating genetically distinct haploid daughter cells. This is facilitated by chromosomes attaching to the nuclear envelope (NE), usually via their telomeres (Kim et al., 2022; Rubin et al., 2020). In vertebrates and many other organisms, the chromosomes move along the inner nuclear membrane (INM) to transiently cluster in a 'meiotic bouquet' (Fig. S1 A) that brings homologues into close proximity and promotes the formation of the synaptonemal complex in zygotene, enhancing synapsis and recombination (Burke, 2018; Kim et al., 2022; Rubin et al., 2020). In many organisms, these dynamic chromosome movements require force generated by the microtubule motor cytoplasmic dynein-1 (dynein, hereafter) either acting directly on the chromosomes (Horn et al., 2013; Lee et al., 2015; Morimoto et al., 2012; Rog and Dernburg, 2015; Sato et al., 2009; Wynne et al., 2012), or indirectly by driving nuclear movement (Burke, 2018; Lee et al., 2015; Rubin et al., 2020). Crucially, the force must be transmitted from the cytoplasm to the chromosomes on the other side of the NE. This is achieved by Linkers of Nucleoplasm and Cytoplasm (LINC) complexes which span the NE to physically connect the cytoskeleton and nucleus (Burke, 2018; Sato et al., 2009; Spindler et al., 2019) (Fig. S1 A).

LINC complexes consist of SUN (Sad1, Unc-84) domain proteins that span the INM, binding nuclear lamins and chromatin associated proteins in the nucleoplasm, and interacting with KASH (**K**larsicht, **A**NC-1, **S**yne **H**omology) domain proteins. KASH proteins have large cytosolic domains that bind cytoskeleton-associated proteins and are anchored in the outer nuclear membrane (ONM) by a C-terminal transmembrane domain (Burke, 2018; Kim et al., 2022; Rubin et al., 2020). Inside the NE lumen, the short C terminal KASH-domain sequence associates with SUN proteins, restricting KASH proteins to the nuclear membrane (Hao and Starr, 2019; Morimoto et al., 2012; Starr and Han, 2002). The meiotic LINC complex can contain SUN1 and SUN2, which have both overlapping and distinct roles in meiosis (Ding et al., 2007; Lei et al., 2009; Link et al., 2014; Schmitt et al., 2007). Although *Sun1*$^{-/-}$ mice are sterile (Chi et al., 2009), SUN2 can recruit telomeres to the NM and drive bouquet formation (Link et al., 2014; Schmitt et al., 2007) and allow some prophase chromosome movement

81 (Lee et al., 2015). SUN1 and 2 bind to a meiotic telomere complex (Dunce et al., 2018;
82 Shibuya et al., 2014) and to KASH5 in vertebrates, or ZYG-12 in C. elegans, which recruit
83 dynein to the ONM (Fig. S1 A) (Horn et al., 2013; Lee et al., 2015; Morimoto et al., 2012; Rog
84 and Dernburg, 2015; Sato et al., 2009; Wynne et al., 2012). KASH5 is essential for
85 mammalian meiosis, as *Kash5*$^{-/-}$ mice are completely sterile due to impaired synapsis,
86 accumulation of double-stranded DNA breaks and resulting meiotic arrest (Horn et al.,
87 2013). Chromosome movement and nuclear rotation in prophase I are also lost (Lee et al.,
88 2015). Human mutations that cause mistargeting of KASH5 to mitochondria lead to male
89 sterility (Bentebbal et al., 2021). KASH5 shares sequence homology with the N-terminal
90 region of the protein encoded by the zebrafish gene *futile cycle* which is required for
91 pronuclear migration (Dekens et al., 2003; Lindeman and Pelegri, 2012), another dynein-
92 dependent function that drives the female pronucleus towards the male pronucleus along
93 microtubules nucleated from the male centrosome (Gönczy et al., 1999; Payne et al., 2003;
94 Reinsch and Karsenti, 1997; Robinson et al., 1999). ZYG-12 performs the same role in C.
95 elegans (Malone et al., 2003), but the KASH protein responsible for pronuclear migration in
96 mammals is not yet known.
97
98 Dynein transports a wide range of cargo to the minus end of microtubules (Reck-Peterson et
99 al., 2018). It is a large 1.6 MDa holoenzyme (Fig. S1 B) comprised of two heavy chains (DHC:
100 DYNC1H1) containing the globular motor domains, which are the site of ATP hydrolysis. Its
101 cargo binding tail domain contains the intermediate chains (ICs: DYNC1I1 and 2) which bind
102 directly to the DHCs; three light chains, which bind to the ICs; and two light intermediate
103 chains (LICs: DYNC1LI1 and 2) (Pfister et al., 2005; Reck-Peterson et al., 2018). The LICs bind
104 to DHC via their N terminal GTPase-like domain which is highly conserved between LICs 1
105 and 2 (Schroeder et al., 2014). The unstructured carboxy terminus protrudes from the
106 motor complex (Celestino et al., 2019; Lee et al., 2018; Schroeder et al., 2014) and is less
107 homologous between LIC1 and 2 apart from two regions of predicted alpha-helix that link
108 dynein to cargo adaptors (Celestino et al., 2019; Kumari et al., 2021b; Lee et al., 2020; Lee et
109 al., 2018).
110
111 Dynein requires the multi-component dynactin complex (Fig. S1 B) for function (Feng et al.,
112 2020; Gill et al., 1991; King et al., 2003; McKenney et al., 2014; Schlager et al., 2014a;

113 Schroer and Sheetz, 1991), although dynein and dynactin alone interact weakly (Baumbach
114 et al., 2017; Chowdhury et al., 2015; Jha et al., 2017; Splinter et al., 2012; Urnavicius et al.,
115 2015). An 'activating adaptor' (Fig. S1 B) is needed for optimum motility and force
116 generation *in vitro* (Belyy et al., 2016; McKenney et al., 2014; Schlager et al., 2014a) (for
117 reviews see (Canty and Yildiz, 2020; Olenick and Holzbaur, 2019; Reck-Peterson et al.,
118 2018)). They strengthen the interaction between dynein and dynactin (Schroeder and Vale,
119 2016; Splinter et al., 2012) by forming extensive interactions with both components to
120 generate a tripartite dynein-dynactin-adaptor (DDA) complex, or complexes with two
121 dyneins per dynactin and adaptor (D_2DA) (Chowdhury et al., 2015; Grotjahn et al., 2018; Lau
122 et al., 2021; Lee et al., 2020; Urnavicius et al., 2018; Urnavicius et al., 2015), or two dyneins,
123 one dynactin and two adaptors (Chaaban and Carter, 2022). Adaptor binding releases the
124 dynein motor domains from the autoinhibited Phi conformation (Torisawa et al., 2014;
125 Zhang et al., 2017), helping to align them for microtubule interaction (Chowdhury et al.,
126 2015; Zhang et al., 2017). Finally, adaptors recruit dynein and dynactin to cargo (e.g.
127 (Horgan et al., 2010b; Schroeder and Vale, 2016; Splinter et al., 2012; Wang et al., 2019)).
128
129 The assembly and function of dynein adaptor complexes is promoted by Lissencephaly-1
130 (LIS1). LIS1 is needed for many dynein functions (Markus et al., 2020) and is mutated in the
131 neurodevelopmental disorder, Type-1 lissencephaly (Reiner et al., 1993). LIS1 binding to the
132 dynein motor domain opens the Phi complex (Elshenawy et al., 2020; Gillies et al., 2022;
133 Htet et al., 2020; Marzo et al., 2020; Qiu et al., 2019) and enhances the formation of DDA
134 complexes (Baumbach et al., 2017; Dix et al., 2013), increasing the frequency, velocity and
135 duration of dynein movement (Baumbach et al., 2017; Dix et al., 2013; Fenton et al., 2021;
136 Gutierrez et al., 2017). LIS1 also increases the proportion of two dynein D_2DA complexes
137 (Elshenawy et al., 2020; Htet et al., 2020) which generate more force, move faster and are
138 more processive than DDA complexes (Elshenawy et al., 2019; Sladewski et al., 2018;
139 Urnavicius et al., 2018). Furthermore, LIS1 contributes to the recruitment of dynein,
140 dynactin and/or adaptors to a wide range of cellular cargoes in interphase and mitosis
141 (Cockell et al., 2004; Dix et al., 2013; Dzhindzhev et al., 2005; Lam et al., 2010; Siller et al.,
142 2005; Sitaram et al., 2012; Splinter et al., 2012; Wang et al., 2013).
143

144 Activating adaptor proteins share little sequence homology, but generally contain a long
145 coiled coil domain, and a site for cargo binding (Lee et al., 2020; McKenney et al., 2014;
146 Redwine et al., 2017; Schlager et al., 2014a; Schlager et al., 2014b; Urnavicius et al., 2015).
147 They bind the C-terminal domain of LICs via at least three distinct types of sequence motif—
148 the CC1 box; the Hook domain; or EF hands (Celestino et al., 2019; Gama et al., 2017; Lee et
149 al., 2020; Lee et al., 2018; Schroeder and Vale, 2016)—and the motility of all three types of
150 complex is promoted by LIS1 (Htet et al., 2020). Other adaptors may not activate dynein,
151 but still link the motor to cargoes (Olenick and Holzbaur, 2019; Reck-Peterson et al., 2018).
152 For example, Rab7-interacting lysosomal protein (RILP) recruits dynein and dynactin to Rab7
153 positive late endosomes/lysosomes (Johansson et al., 2007; Jordens et al., 2001; Scherer et
154 al., 2014; Tan et al., 2011) via its RILP homology domains, but lacks a long coiled coil. The
155 KASH proteins KASH5 and ZYG-12 are good activating adaptor candidates, because they bind
156 dynein, have long coiled coils, with KASH5 having an N-terminal EF hand domain (Horn et
157 al., 2013; Morimoto et al., 2012) whereas ZYG-12 has a Hook domain (Malone et al., 2003).
158 However, unlike other activating adaptors identified so far, they are trans-membrane
159 proteins.
160
161 Mammalian dynein contains either two LIC1 subunits, or two LIC2 subunits (Tynan et al.,
162 2000a), providing the potential for differential interactions with adaptors. However, both
163 LICs bind to the adaptors Rab11-FIP3 (Celestino et al., 2019; Horgan et al., 2010a; Horgan et
164 al., 2010b), RILP (Celestino et al., 2019; Scherer et al., 2014), BICD2, spindly, Hook3, ninein
165 and TRAK1 (Celestino et al., 2019), via the highly conserved helix 1 in the LIC C-terminus.
166 This shared binding ability suggests that LICs may act redundantly, as has been reported in
167 the endocytic pathway (Horgan et al., 2010a; Horgan et al., 2010b; Tan et al., 2011).
168 However, other endocytic functions may be isoform-specific (Bielli et al., 2001; Hunt et al.,
169 2013; Palmer et al., 2009). Likewise, although LIC1 and 2 act redundantly for some mitotic
170 functions (Jones et al., 2014; Raaijmakers et al., 2013), isoform-specific functions and
171 localisations have been reported in mitosis (Horgan et al., 2011; Mahale et al., 2016a;
172 Mahale et al., 2016b; Palmer et al., 2009; Raaijmakers et al., 2013; Sharma et al., 2020;
173 Sivaram et al., 2009), at the centrosome (Tynan et al., 2000b), during neuronal nuclear
174 migration (Goncalves et al., 2019) and cell migration (Even et al., 2019; Schmoranzer et al.,
175 2009). In addition, mitotic phosphorylation of the LIC1 C-terminal domain may offer

176 temporal control of adaptor selection (Kumari et al., 2021a). The degree of specific and
177 shared functions for LICs is an important issue that is not fully resolved.
178
179 How the dynein motor interacts with KASH5 to drive the dynamic chromosome movements
180 essential for mammalian meiosis has been poorly understood. Here, we reveal KASH5 to be
181 a dynein activating adaptor that interacts with the LIC helix 1 region, in agreement with
182 recent work (Agrawal et al., 2022). We show that this region in the LIC is also key for
183 dynein's function at the Golgi apparatus and throughout the endocytic pathway, with LICs 1
184 and 2 acting redundantly. Analysis of the hierarchy of adaptor complex assembly reveals
185 that dynein can be recruited to KASH5 independently of dynactin, and that LIS1 is essential
186 for full complex assembly. The interaction between KASH5 and dynein is disrupted by
187 mutation of the KASH5 EF hand domain, although dynein recruitment to KASH5 in cells is
188 calcium independent. Since defective synapsis can lead to genetic abnormalities and
189 infertility, the characterisation of the KASH5-dynein interaction is an important step forward
190 in understanding the complex mechanism of chromosome movement during mammalian
191 meiotic prophase I.
192
193 **Results**
194 **KASH5 forms a complex with dynein, dynactin and LIS1**
195 Because KASH5 is expressed only in the meiotic germ line, HeLa cells provide a convenient
196 "KASH5-null" background for studying the interaction between dynein and KASH5 (Horn et
197 al., 2013; Morimoto et al., 2012). We generated a stable HeLa cell line in which expression
198 of GFP-KASH5 was induced by doxycycline so that the recruitment of endogenous dynein
199 and dynactin to the nuclei of KASH5-expressing cells could be visualised by
200 immunofluorescence. LIC1 and dynactin p50 were both recruited to KASH5-expressing
201 nuclei (Fig. 1 A), in addition to dynactin p150 and IC (Horn et al., 2013). In contrast, neither
202 dynein nor dynactin were recruited to the nuclei of cells transiently expressing a different
203 KASH protein, nesprin-2α2 (GFP-N2α2).
204
205 We confirmed the recruitment of dynein and dynactin to KASH5 biochemically. HeLaM cells
206 were transiently transfected with GFP-KASH5ΔK (Fig. 1 B) or GFP-N2α2ΔK, which lack their
207 KASH and transmembrane domains, and so are cytosolic. LIC1, LIC2, IC and p150 all

208 associated with GFP-KASH5ΔK and not with GFP-N2α2ΔK (Fig. 1 C). The KASH5 N-terminal
209 166 amino acids (GFP-KASH5ND), containing the EF-hands, was able to pull down dynein IC
210 and dynactin from cell lysates (Horn et al., 2013), and we found that it was somewhat more
211 efficient than GFP-KASH5ΔK for LIC1 (Fig. 1 D), as seen for IC (Horn et al., 2013).
212
213 LIS1 plays a key role in the assembly of DDA and D_2DA complexes (reviewed in (Canty and
214 Yildiz, 2020; Markus et al., 2020; Olenick and Holzbaur, 2019), and co-precipitates with
215 BICD2N, dynein and dynactin (Splinter et al., 2012). As reported previously (Horn et al.,
216 2013), GFP-KASH5ΔK pulled down LIS1 as well as dynein and dynactin, but this complex
217 excluded the dynein adaptor BICD2 (Fig. 1 C). Immunofluorescence analysis revealed that
218 endogenous LIS1 was detected at the NE in 99.8% of KASH5-expressing cells (Fig. 1 A; Fig. S1
219 C), whereas the LIS1 and dynein interactor Nde1 was not, even though it could be detected
220 at the NE in late G2 cells (Fig. 1 A).
221
222 **Hierarchy of dynein, dynactin and LIS1 recruitment to KASH5**
223 We next sought to identify which dynein subunits mediate the KASH5 interaction, and the
224 roles played by dynactin and LIS1. We used RNA interference to deplete individual dynein
225 subunits in the GFP-KASH5 cell line (Fig. S2 A) and assessed the effect on recruitment to
226 KASH5. Depletion of dynein IC2 (the only form expressed in HeLa cells: (Palmer et al., 2009))
227 did not prevent dynein recruitment (Fig. 2 A), with 100% of KASH5-positive nuclei being
228 labelled with anti-LIC1 (Fig. S1 C). Cytosolic levels of LIC1 were reduced following IC2
229 depletion, making the NE pool particularly distinct. This is likely due to a modest reduction
230 in total dynein levels when IC2 is depleted, as seen by immunoblotting with anti-LIC1 and 2
231 (Fig. S2 A). LIS1 recruitment to KASH5 at the NE was also unaffected by depletion of IC2 (Fig.
232 2 A and S1 C). Strikingly, dynactin was only rarely detected at the NE in IC2-depleted cells
233 using antibodies to p150 or p50 (Fig. 2 A and S1 C), even though p150 was still readily
234 observed at microtubule plus ends. These data suggest that while the interaction between
235 IC and p150 (Karki and Holzbaur, 1995; King et al., 2003; Vaughan and Vallee, 1995) is not
236 needed for dynein and LIS1 recruitment to KASH5, it is essential for the association of
237 dynactin with KASH5.
238

239 Since IC2 depletion reduced total cellular dynactin p150 levels by ~25% (Fig. S2 A), we used
240 a dominant negative approach as another way of testing the effect of disrupting IC2-p150
241 interactions on recruitment to KASH5, using over-expression of the coiled coil 1 region of
242 p150 (CC1) (King et al., 2003; Quintyne et al., 1999). Unfortunately, transiently transfected
243 constructs would not co-express with GFP-KASH5 in the inducible GFP-KASH5 cell line. We
244 therefore transiently co-transfected HeLa cells with GFP-KASH5 and myc-SUN2 (to enhance
245 localisation of KASH5 to the NE) along with RFP-tagged CC1. Notably, while CC1 expression
246 had no effect on dynein or LIS1 recruitment to KASH5, it prevented dynactin accumulation
247 at the NE (Fig. 2 B), confirming that dynein and LIS1 can associate with KASH5 independently
248 of dynactin.
249
250 We used RNAi to investigate the involvement of LICs in the dynein-KASH5 interaction. There
251 was no reduction in the proportion of cells with detectable dynein, dynactin or LIS1
252 recruited to KASH5 after depleting LIC2 alone (Fig. 3 B, D). LIC1 depletion also had very little
253 effect on dynactin or LIS1 recruitment in a binary scoring assay, but had a variable effect on
254 dynein intermediate chain, with 80.8 ± 24.3% of cells (n=3 experiments, ±SD) showing IC
255 signal at the NE (Fig. 3 A, D). However, when both LIC1 and LIC2 were depleted
256 simultaneously, the proportion of cells with detectable dynein and dynactin at the NE was
257 reduced by ~75% (Fig. 3 C, D). LIS1 recruitment was also reduced, with ~40% of KASH5
258 expressing cells showing no LIS1 signal at the NE. We were not able to deplete endogenous
259 LIC1 completely using RNAi (Fig. S2 B) which may explain why in some cells a residual level
260 of dynein, dynactin and LIS1 remained with KASH5. In addition, GFP-KASH5ΔK pull-downs
261 from LIC1 and 2 depleted HeLa cells contained very little dynein and dynactin (Fig. 3 E).
262 Thus, LIC1 and 2 act redundantly to recruit dynein and LIS1 to KASH5 at the NE, with
263 dynactin being recruited downstream, by a mechanism requiring the interaction between IC
264 and p150.
265
266 To test if LIS1 is required for KASH5 to associate with dynein and dynactin, we depleted LIS1
267 using RNAi. Interestingly, the proportion of cells with LIC1 detectable at the NE was virtually
268 unaffected by LIS1 knock-down (Fig. S1 D, E) whereas p150 recruitment was seen in only
269 20% of cells (Fig. S1 D, G). Dynein IC detection at KASH5-positive nuclei varied between
270 experiments (Fig. S1 D, F), with a mean of 57.1% of cells positive for IC74 antibody labelling.

271 The discrepancy between the anti-LIC1 and IC scoring most likely reflects the weaker NE
272 labelling seen with the IC74 antibody compared to anti-LIC1 antibodies in control cells. Our
273 interpretation of these data is that LIS1 depletion reduces dynein levels at the NE
274 somewhat, to levels that are still detectable by anti-LIC1 but sometimes not by IC74.
275 Altogether, these data reveal that LIS1 is vital for the dynactin complex to be recruited to
276 KASH5 downstream of dynein and suggest that LIS1 may also promote the formation of, or
277 stabilise, the KASH5-dynein complex.
278
279 **Dynein LIC1 helix 1 is essential for KASH5 binding**
280 We next wanted to ascertain the LIC1 region responsible for the dynein-KASH5 interaction.
281 Assays with purified protein have shown that helix 1 and some preceding amino acids (433-
282 458) was the minimal LIC1 region needed for interaction with Hooks, BICD2 and Spindly (Lee
283 et al., 2018), with additional interactions between LIC1 and Spindly, BICD2 and Hook3 being
284 seen in helix 2 and the linker region upstream of helix 1 (Celestino et al., 2019). In contrast,
285 RILP required only helix 1 (LIC1 440-455) (Celestino et al., 2019). We made a series of hLIC1
286 constructs (Fig. 4 A): full length LIC1; a truncation containing helix 1 but not helix 2 (LIC1-
287 CT2: amino acids 1-456); and a construct which terminates shortly after the Ras-like domain
288 and lacks both helices and the linker sequences (LIC1-CT3: amino acids 1-388). Cells
289 depleted of LIC1 and 2 by RNAi were co-transfected with myc-tagged LIC1 constructs and
290 the soluble GFP-KASHND. GFP trap IP revealed that while dynein containing LIC1-FL and
291 LIC1-CT2 was recruited to the KASH5 N-terminal domain, dynein with LIC1-CT3 was not (Fig.
292 4 B). Previous work has shown that deletion of just helix 1 (N440-T456) or helix 1 point
293 mutants (F447A/F448A and L451A/L452A) prevented binding of the LIC1 C-terminal domain
294 to several dynein adaptors using purified proteins (Celestino et al., 2019). We generated the
295 helix 1 deletion and mutations in GFP-LIC1 (Fig. 4A), and also a deletion lacking helix 1 plus
296 some linker sequence (S433-S458). These were co-expressed with HA-tagged KASH5ΔK in
297 HeLaM cells depleted of both LICs. Full length GFP-LIC1 pulled down KASH5ΔK effectively,
298 whereas the LIC1 helix 1 deletions and point mutants did not (Fig. 4C). We then examined
299 the recruitment of LIC1 to KASH5 at the NE in HeLaM cells co-expressing HA-KASH5, myc-
300 SUN2 and GFP-LIC1 constructs. Both wild-type GFP-LIC1 and the mid-length LIC1-CT2 were
301 recruited to KASH5, although CT2 detection at the NE was variable (Fig. 4 D, E). In contrast,

302 LIC1-CT3, the helix 1 deletions, and helix 1 point mutants were poorly recruited. Altogether,
303 these results demonstrate LIC1 helix 1 is essential for interaction with KASH5.
304
305 The importance of LIC helix 1 in cargo binding prompted us to assess the role of the LICs on
306 endogenous membrane cargoes, whose adaptors have not been fully defined. First, we
307 tested if LIC1 and 2 functioned redundantly in Golgi apparatus morphology and positioning,
308 for which there is conflicting published evidence (Kumari et al., 2021a; Palmer et al., 2009;
309 Tan et al., 2011). RNAi depletion of LIC1 or 2 individually led to break-up of the Golgi ribbon
310 in ~60% of HeLaM cells, with the Golgi fragments remaining centrally located (Fig. 5 A-C). In
311 contrast, depletion of both LICs simultaneously led to complete fragmentation and
312 scattering of the Golgi apparatus (Fig. 5 B, C), demonstrating that the LICs act redundantly in
313 Golgi positioning. This was confirmed by expressing RNAi-resistant LIC1-mKate or LIC2-
314 mKate in cells depleted of both LICs (Fig. 5 D), as either LIC was able to fully restore Golgi
315 apparatus clustering. The endocytic pathway also relies heavily on dynein activity (Flores-
316 Rodriguez et al., 2011; Granger et al., 2014; Reck-Peterson et al., 2018; Wang et al., 2019),
317 which contributes to the sorting of endocytic cargo in the early endosome (Driskell et al.,
318 2007). Depletion of both LICs profoundly altered the distribution of early endosomes,
319 recycling endosomes and lysosomes (Fig. S3 A) while only minimal effects were seen with
320 single depletions (not shown). Moreover, expression of either LIC1-mKate or LIC2-GFP
321 restored the position of endocytic organelles (Fig. S3 B), confirming that LICs act
322 redundantly in this context. We investigated if the same effects were observed with dynein
323 recruitment to RILP. Recruitment of dynein and dynactin to HA-RILP-positive late
324 endosomes was significantly reduced when both LICs were depleted together, but not
325 individually (Fig. S4 A-D).
326
327 To examine if the LIC1 region 388-456 that contains helix 1 is needed for Golgi apparatus
328 and endocytic organelle positioning, we used our knock-down and rescue approach (Figs. 5
329 E; S3 C, D; S4 E). Both full length GFP-LIC1 and GFP-LIC1-CT2 rescued Golgi apparatus, early
330 endosome, and lysosome clustering. In contrast, GFP-LIC1-CT3 did not, with EEA1-positive
331 early endosomes (Fig. S3 C) and LAMP1-positive late endosomes/lysosomes (Fig. S3 D)
332 remaining localised in the cell periphery, and the Golgi apparatus being fragmented and

333 scattered (Fig. 5 E). Moreover, GFP-LIC1-CT3 did not interact with RILP, whereas GFP-LIC1-
334 CT2 or full-length GFP-LIC1 were robustly recruited to RILP positive organelles (Fig. S4 E).
335
336 Altogether, these data provide clear *in cellulo* evidence that the LIC adaptor binding helix 1
337 is needed for dynein's interaction with KASH5 and RILP, and is also crucial for dynein's
338 function on the Golgi apparatus, early endosomes and lysosomes. Furthermore, we
339 demonstrate that LIC1 and LIC2 act redundantly in these situations.
340
341 **KASH5 is a novel activating dynein adaptor**
342 KASH5 shares key properties with other activating dynein adaptors: interaction with LIC
343 helix 1; ability to recruit dynactin; and presence of an N-terminal dynein binding domain
344 (containing EF-hands) followed by an extended coiled coil (Horn et al., 2013). In addition,
345 KASH5's biological function in telomere clustering in prophase of meiosis I (Horn et al.,
346 2013; Lee et al., 2015) strongly suggest that it recruits active dynein. When expressed out of
347 its meiotic context, in HeLa cells, we quite often observed clusters of KASH5 and dynein
348 around discrete points close to or on top of the nucleus (red arrowheads and arrows in Fig.
349 1 A), suggestive of clustering around the centrosome via active dynein. In addition,
350 asymmetric distribution of KASH5 in the NE with enrichment towards the MTOC has been
351 noted (Horn et al., 2013).
352
353 Overexpression of activating dynein adaptor proteins lacking their cargo binding domain
354 disrupts dynein functions by sequestering dynein and preventing its binding to endogenous
355 adaptors (e.g. (Hoogenraad et al., 2001; Hoogenraad et al., 2003; Horgan et al., 2010a;
356 Horgan et al., 2010b; Splinter et al., 2012). As KASH5 interacts with LIC helix 1, we
357 hypothesised that it would compete with other adaptors for binding to dynein. Indeed,
358 overexpression of cytosolic GFP-KASH5ΔK in HeLaM cells resulted in complete
359 fragmentation of the Golgi apparatus, and redistribution of lysosomes to the cell periphery;
360 phenotypes indicative of a loss of dynein function (Fig. 6 A). In contrast, expression of a
361 cytoplasmic KASH5 construct lacking its N terminal dynein binding domain (Fig. 1 B, GFP-
362 KASH5ΔNDΔK (Horn et al., 2013)) had no effect on Golgi apparatus or lysosome distribution
363 and morphology (Fig. 6 A). The effects of GFP-KASH5ΔK are therefore due to KASH5 binding
364 and sequestering dynein, preventing its recruitment to other membrane cargoes.

365

366 We next determined if KASH5 competes with established dynein adaptors for dynein
367 binding. To test this possibility, we co-transfected HeLaM cells with HA-tagged full-length
368 KASH5, myc-tagged SUN2 and dominant negative versions of the activating adaptors BICD2
369 (GFP-BICD2N: (Hoogenraad et al., 2001; Splinter et al., 2012)) and Rab11-FIP3 (GFP-Rab11-
370 FIP3 I737E, which retains its LIC binding domain but is unable to interact with Rab11 (Wilson
371 et al., 2005)). Endogenous dynein was recruited to KASH5 at the NE in control cells, but this
372 was prevented when dominant negative dynein adaptors BICD2N and Rab11-FIP3 I737E
373 were expressed (Fig. 6 B). We investigated if the same was true for dynein recruitment to
374 RILP, even though RILP is not thought to be able to activate dynein/dynactin motility (Lee et
375 al., 2020; Reck-Peterson et al., 2018). Dynein was recruited to RILP-positive organelles
376 following overexpression of HA-tagged RILP (Fig. 6 C). However, when GFP-BICD2N or GFP-
377 Rab11-FIP3 I737E were co expressed, recruitment of dynein LIC1 to RILP was abrogated (Fig.
378 6 C). Taken together, these findings show that established dynein adaptor proteins compete
379 with KASH5 and RILP for dynein binding.
380

381 To test directly if KASH5 could act as an activating adaptor and form motile complexes with
382 dynein and dynactin, we used single molecule in vitro motility assays consisting of purified
383 bacterially expressed KASH5 truncations (Fig. 7 A) mixed with purified fluorescently-labelled
384 dynein, dynactin and LIS1. We generated three KASH5 constructs encoding amino acids 1-
385 407, 1-460, 1-507, all of which contain the N-terminal EF-hand dynein binding domain plus
386 the predicted coiled coil region (amino acids 166-350), plus a variable amount of the C-
387 terminal region. SEC-MALS analysis showed that all three proteins formed dimers (Fig. 7 B).
388 Of these, $KASH5_{1-460}$ was the most active in motility assays using dynein containing a heavy
389 chain mutant that cannot form the inhibited Phi conformation (Zhang et al., 2017) (Fig. 7C).
390 We next used assays with wild type purified dynein, which when combined with dynactin
391 and LIS1 alone displayed very little motility (Fig. 7 D). The inclusion of $KASH5_{1-460}$ promoted
392 processive dynein movements (Fig. 7 D, E), although a lesser number than seen with
393 purified $Hook3_{1-522}$ (Urnavicius et al., 2018). KASH5 EF-hands (amino acids 1-115), the coiled
394 coils (amino acids 155-349), or a combination of EF-hands and coiled coils alone (amino
395 acids 1-349) were not enough to activate dynein/dynactin (Fig. 7 F). Importantly, the

396 velocity of processive dynein movements was the same for $KASH5_{1-460}$ and $Hook3_{1-522}$ (Fig. 7
397 E). KASH5, a transmembrane protein, is therefore an activating dynein adaptor.
398
399 **KASH5's EF hand is critical for dynein and dynactin complex assembly**
400 A common feature of several dynein adaptor proteins is the presence of an N terminal pair
401 of EF hands in the dynein-binding domain, as seen in Rab11-FIP3, CRACR2a, Rab45/RASEF
402 and ninein (Celestino et al., 2019; Lee et al., 2020; Reck-Peterson et al., 2018; Wang et al.,
403 2019). KASH5 contains two putative EF hands, extending from amino acids 36-103, which
404 form the bulk of the dynein binding domain (Fig. 1 B, D; 4 C). Sequence alignment of the
405 KASH5 EF hands with CRACR2a, Rab45, FIP3 and ninein revealed that KASH5, like FIP3 and
406 ninein, lacks some key consensus calcium-binding amino acids (at positions X,Y,Z,-X,-Y,-Z),
407 with these changes being consistent across species (Fig. 8 A). EF hand 1 is particularly
408 divergent, with only the residue in position X (Grabarek, 2006) matching the consensus, and
409 with the key position -Z being a glutamine or histidine instead of a glutamate residue. While
410 EF hand 2 has consensus amino acids in position X, other residues either do not conform or
411 vary between species. For example, in non-rodent KASH5 EF hand 2, there is aspartate in
412 place of glutamate at -Z, which can result in magnesium binding (Grabarek, 2006), as
413 suggested for FIP3 (Lee et al., 2020).
414
415 This analysis suggested that KASH5 might not be calcium regulated. To determine if the
416 KASH5 and Rab11-FIP3 interaction with dynein in cells required calcium or not, we
417 expressed GFP-tagged KASH5 with myc-SUN2 in HeLaM cells, or GFP-Rab11-FIP3 in Vero
418 cells, and labelled for endogenous LIC1. In control DMSO-treated cells there was robust
419 recruitment of dynein to KASH5 at the NE and to Rab11-FIP3-positive recycling endosomes
420 (Fig. S5). This recruitment was not affected by treating cells with the cell permeable calcium
421 chelator, BAPTA-AM, for 2 hours to deplete intracellular calcium (Fig. S5). Furthermore,
422 endogenous LIC1 was present at equal levels when GFP-KASH5-ND was pulled down from
423 cell lysates in the presence or absence of EGTA (Fig. 8 B). This demonstrates that the KASH5-
424 dynein interaction does not require calcium and confirms that the Rab11-FIP3-dynein
425 interaction in cells is calcium-independent, as reported for in vitro assays (Lee et al., 2020).
426

427 We wanted to test the importance of KASH5's EF hands in the dynein interaction, even if
428 calcium was not required. The *fue* mutation in the zebrafish KASH5 homologue, futile cycle
429 (fue) (Lindeman and Pelegri, 2012), gives zygotes that are defective in pronuclear migration
430 and mitotic spindle assembly (Dekens et al., 2003; Lindeman and Pelegri, 2012). The
431 corresponding mutation in human KASH5 changes a valine to glutamic acid in EF hand 1
432 (V54E: Fig. 8 A). We generated KASH5-EF-*fue* constructs to establish how this mutation
433 affected KASH5-dynein interactions. We also mutated the amino acids in positions X and Y
434 of both EF hands to alanine (KASH5-EF-AA: D44A; Q46A; D81A; N83A: Fig. 8 A), as these
435 mutations in CRACR2a ablate its function (Srikanth et al., 2016; Wang et al., 2019). Lastly,
436 we replaced some KASH5 residues by those found in CRACR2a (Fig. 8 A). KASH5-EF-mod1
437 has four substitutions: Q46E; Q55D; P87Y and K88L. In KASH5-EF-mod2, nine amino acids in
438 EF hands 1 and 2 and part of the exiting helix were changed to the CRACR2a sequences.
439
440 To test which KASH5 mutants could form a stable complex with dynein and dynactin, GFP-
441 KASH5ΔK-WT or EF hand mutants were isolated from HeLaM cells by GFP-trap and probed
442 for endogenous IC and dynactin p150. Unmodified GFP-KASH5ΔK co-precipitated with
443 dynein and dynactin, as did GFP-KASH5ΔK-EF-mod1 (Fig. 8 B). Interestingly, dynein
444 recruitment to EF-mod1 was greater than to KASH5ΔK-WT in 2/3 experiments. In contrast,
445 much less dynein and dynactin bound to the GFP-KASH5ΔK-EF-*fue*, EF-AA, or EF-mod2
446 mutants. In agreement, we found that endogenous dynein was recruited to full length GFP-
447 KASH5 and GFP-KASH5-EF-mod-1 at the NE, whereas GFP-KASH5-EF-*fue*, EF-AA, or EF-mod2
448 mutants did not accumulate dynein (Fig. 8 C and D).
449
450 As another means of assessing the effects of these mutations on KASH5-dynein binding, we
451 harnessed the dominant negative effect of expressing cytosolic KASH5, which causes Golgi
452 fragmentation by sequestering dynein (Fig. 6A). In this assay, any mutant that prevents
453 KASH5 from binding dynein would have no effect on Golgi morphology when expressed, as
454 seen with GFP alone (Fig. 8 E). Overexpression of GFP-KASH5ΔK or GFP-KASH5ΔK-mod1 in
455 HeLaM cells resulted in strong fragmentation of the Golgi apparatus. In contrast, GFP-
456 KASHΔK-EF-*fue*, GFP-KASHΔK-EF-AA or GFP-KASHΔK-EF-mod2 (Fig. 8 E) had a much weaker
457 effect on Golgi positioning, implying that these EF hand mutants were much less able to

458 sequester dynein. Altogether, these findings show that the KASH5 EF hand is critical for its
459 function with dynein and dynactin, although the interaction is not calcium dependent.
460
461 **Discussion**
462 Infertility will affect approximately 1 in 7 couples trying to conceive and has extraordinarily
463 detrimental effects on those affected. Despite this, surprisingly little is known about the
464 multitude of molecular and genetic causes of infertility. This is largely due to the complexity
465 of meiosis and pronuclear migration, and a lack of samples to study from sterile
466 populations. Dynein generates the mechanical force required for the dynamic chromosome
467 movements in meiotic prophase I that are essential for meiotic progression and to maintain
468 genetic integrity. KASH5 is part of the mammalian LINC complex component that spans the
469 NE to link dynein to telomeres and is essential for synapsis and meiotic progression (Horn et
470 al., 2013; Morimoto et al., 2012). Here, we show that KASH5 is a trans-membrane activating
471 adaptor for dynein, in agreement with a recent report (Agrawal et al., 2022). We reveal that
472 dynein-KASH5 interactions require LIC helix 1 (LIC1 residues 440-456), which mediates
473 dynein's interaction with many other cargo adaptors (Celestino et al., 2019; Lee et al., 2020;
474 Lee et al., 2018). Accordingly, KASH5 competes with established dynein adaptors for dynein
475 binding, and expression of a cytosolic KASH5 truncation inhibits dynein interphase function
476 (Fig. 6), as seen for other dynein adaptor constructs that cannot bind cargo (Hoogenraad et
477 al., 2001; Hoogenraad et al., 2003; Horgan et al., 2010a; Horgan et al., 2010b; Splinter et al.,
478 2012). Our *in vitro* assays (Fig. 7) confirm that KASH5 is an activating dynein adaptor
479 (McKenney et al., 2014; Schlager et al., 2014a; Schlager et al., 2014b) as KASH5, in the
480 presence of LIS1 and dynactin, promotes motility of purified dynein molecules (Fig. 7), as
481 recently reported (Agrawal et al., 2022).
482
483 Considerable force must be exerted to move chromosomes within the nucleoplasm to
484 promote synapsis. There may be ~80 LINC complexes per telomere (Spindler et al., 2019),
485 each providing a point where dynein motors can engage with the cytoplasmic face of the
486 NE. A key question is how many dyneins bind to each LINC complex, which likely contains
487 three KASH5 dimers bound to two SUN trimers (Gurusaran and Davies, 2021). Solution
488 studies suggest that a single LIC protein binds per KASH5 dimer (Agrawal et al., 2022), in
489 keeping with the report that two BICD2 proteins can assemble with one dynactin and two

490 dyneins (Chaaban and Carter, 2022), with the LICs from one of the dyneins interacting with
491 both of the BICD2 adaptors. This suggests that there maybe one or two dyneins per LINC
492 complex, and an ensemble of 80-160 dyneins per telomere.
493
494 Importantly, we find that KASH5 recruits LIS1 as well as dynein and dynactin. LIS1 is crucial
495 for dynein function where high force is needed (Chapman et al., 2019; Markus et al., 2020;
496 Pandey and Smith, 2011; Reddy et al., 2016; Yi et al., 2011). It increases dynein force
497 generation in vitro by promoting the recruitment of two dynein motors per dynactin
498 (Elshenawy et al., 2020; Htet et al., 2020; Markus et al., 2020) and opens the dynein phi
499 complex to allow easier assembly of the dynein/dynactin/adaptor complex (Elshenawy et
500 al., 2020; Gillies et al., 2022; Htet et al., 2020; Marzo et al., 2020; Qiu et al., 2019). Indeed, in
501 cells, LIS1 enhances dynein and dynactin recruitment to a wide range of cellular cargoes,
502 including the NE in late G2 (Cockell et al., 2004; Dix et al., 2013; Dzhindzhev et al., 2005; Lam
503 et al., 2010; Siller et al., 2005; Sitaram et al., 2012; Splinter et al., 2012; Wang et al., 2013).
504 Our data suggest that LIS1 is essential for recruiting dynactin to KASH5 (Fig. S1). Surprisingly,
505 LIS1 depletion had much less effect on dynein recruitment. We also saw that interfering
506 with dynein IC-p150 interactions by IC2 depletion or over-expression of p150 CC1 did not
507 prevent dynein recruitment to KASH5. Based on these data, we propose that the first step in
508 KASH5 adaptor complex assembly is an interaction between LIC helix 1 and the KASH5 EF-
509 hands. Next, binding of LIS1 opens the dynein phi complex. The third step involves
510 recruitment of the dynactin complex initiated by the IC-p150 interaction, followed by the
511 formation of extensive contacts between the dynactin complex and the adaptor
512 (Chowdhury et al., 2015; Grotjahn et al., 2018; Lau et al., 2021; Lee et al., 2020; Urnavicius
513 et al., 2018; Urnavicius et al., 2015; Zhang et al., 2017). Interestingly, forming the active
514 complex requires more than just the KASH5 EF-hands and coiled coil region (amino acids 1-
515 349, Fig. 7). There is a potential spindly motif (Gama et al., 2017) at amino acids 371-376
516 (Agrawal et al., 2022), which in other adaptors interacts with the pointed end of dynactin
517 (Chaaban and Carter, 2022; Lau et al., 2021). This motif is present in all motility-promoting
518 KASH5 truncations (Fig. 7).
519
520 An interesting question is whether dynein's conformation (phi or open) affects its ability to
521 bind adaptors, or subsequently recruit dynactin. If so, then LIS1 binding may regulate

522 adaptor complex assembly *per se*. While LIS1 does not remain in motile complexes with
523 dynein and dynactin in vitro (Elshenawy et al., 2020; Htet et al., 2020), it appears to be a
524 stable component of at least some DDA complexes in vivo because it is recruited to KASH5
525 at the NE. It is also found along with dynein and dynactin in KASH5 (Fig. 1; (Horn et al.,
526 2013)) and BICD2 pull-downs (Splinter et al., 2012). It is also required for dynein-dynactin
527 recruitment to the NE in late G2/prophase (Raaijmakers et al., 2013). Understanding fully
528 the in vivo role of LIS1 in dynein-dynactin-adaptor function is a key challenge for the future.
529
530 KASH5 interacts with LICs via its N-terminal EF-hand domain, like FIP3, CRACR2a, Rab45 and
531 ninein (Celestino et al., 2019; Lee et al., 2020; Reck-Peterson et al., 2018; Wang et al., 2019).
532 Many EF-hands are known for their regulation by calcium, and CRACR2a-dynein interactions
533 are calcium-dependent (Wang et al., 2019). However, not all EF hand adaptors bind calcium,
534 nor does calcium binding necessarily regulate EF hand function (Lee et al., 2020; Wang et
535 al., 2019). Indeed, neither KASH5-dynein nor FIP3-dynein interactions were affected by
536 calcium depletion (Fig. S5), and the KASH5 EF-hands lack key residues known to be essential
537 for calcium binding (Fig. 8 A). Furthermore, helix 1 peptide binding to purified KASH5 was
538 not calcium sensitive, and KASH5 did not bind calcium (Agrawal et al., 2022). However, the
539 structure of the KASH5 EF-hand is clearly vital, since mutating the X and Y positions of both
540 EF-hands to alanine ablated KASH5-dynein interactions (Fig. 8). Similar adverse effects on
541 dynein-KASH5 association were seen after mutation of other residues in KASH5 EF-hands,
542 and the expression of one of these (L147D) reduced the levels of dynactin somewhat at
543 telomeres in mouse spermatocytes in vivo (Agrawal et al., 2022). Importantly, our studies
544 suggest why the *fue* mutation in the EF-hand (Lindeman and Pelegri, 2012) is detrimental in
545 zebrafish development (Dekens et al., 2003; Lindeman and Pelegri, 2012). It puts a
546 negatively charged glutamic acid in place of a hydrophobic valine in the first exiting helix,
547 which disrupts KASH5-dynein interactions in vitro and in cells (Fig. 8). Interestingly, zebrafish
548 *fue* mutants are defective in pronuclear migration (Dekens et al., 2003). Similarly, Zyg12, the
549 *C. elegans* LINC complex KASH-domain protein that binds dynein LIC via a Hook domain, is
550 needed for both pronuclear migration (Malone et al., 2003; Minn et al., 2009) and meiotic
551 synapsis (Sato et al., 2009). Whether KASH5 plays a role in mammalian pro-nuclear
552 migration remains to be determined.
553

554 As well as characterising KASH5 as a dynein adaptor, we also provide insight into LIC
555 function in cells. Either LIC can recruit dynein to KASH5 in cells (Fig. 3), as confirmed by using
556 pull-downs with GFP-LIC1 (Figs. 4, 8) and reconstituting KASH5-activated motility of dynein
557 containing only LIC2 (Fig. 7). Similarly, LICs 1 and 2 act redundantly for recruitment of dynein
558 to RILP, and in the positioning of the Golgi apparatus and recycling, early and late
559 endosomes in cells (Figs. 5 and S3). We also show that the helix 1-containing region is
560 essential for all these roles. This is in keeping with roles for Hooks and BicD2 at the Golgi
561 apparatus (Christensen et al., 2021; Hoogenraad et al., 2001; Hoogenraad et al., 2003;
562 Splinter et al., 2012), and Hooks (Christensen et al., 2021; Guo et al., 2016; Olenick et al.,
563 2019; Villari et al., 2020), FIP3 (Horgan et al., 2010a; Horgan et al., 2010b) and RILP
564 (Johansson et al., 2007; Jordens et al., 2001; Scherer et al., 2014; Tan et al., 2011) in
565 endocytic organelle dynamics, since all of these adaptors can interact with both LICs
566 (Celestino et al., 2019; Christensen et al., 2021; Lee et al., 2020; Lee et al., 2018; Schlager et
567 al., 2014a; Schroeder et al., 2014; Schroeder and Vale, 2016; Urnavicius et al., 2018),
568 although BicD2 may preferentially bind LIC1 in vivo (Goncalves et al., 2019). As yet,
569 however, there is no molecular explanation for why LIC1 is needed for motility of SNX8-
570 labelled endosomal tubules whereas LIC2-dynein moves SNX1 and SNX4 tubules (Hunt et al.,
571 2013). Other isoform-specific roles for LICs have been described (see introduction),
572 particularly in mitosis, where LIC phosphorylation, coupled with Pin1 binding, may help
573 control which adaptors bind to LIC1 and LIC2 (Kumari et al., 2021a; Kumari et al., 2021b). LIC
574 phosphorylation, included in the region just upstream of helix 1, also plays a key role in
575 switching dynein from interphase to mitotic cargos (Addinall et al., 2001; Dwivedi et al.,
576 2019; Kumari et al., 2021a; Niclas et al., 1996).
577
578 Altogether, we have shown that KASH5 is a novel trans-membrane member of the dynein
579 activating adaptor protein class, mapped its interaction with dynein LICs, and demonstrated
580 that the KASH5 EF hands are critical for this process. This work also sheds light on order in
581 which dynein-dynactin-adaptor complexes assemble in cells, and the involvement of LIS1 in
582 this process.

583 **Materials and Methods**

584 **Antibodies and constructs**

585 The following mouse antibodies were used: dynein IC (IC74, MAB1618, Millipore;
586 RRID:AB_2246059); EEA1 (Clone 14, BD Biosciences; RRID:AB_397830); LAMP1 (Clone H4A3,
587 Developmental Studies Hybridoma Bank, RRID:AB_2296838; or Abcam, RRID:AB_470708);
588 LIS1 (Sigma-Aldrich L7391; RRID:AB_260418); dynactin p150 (BD Transduction Laboratories
589 610473; RRID:AB_397845); GFP (Roche 11814460001; RRID:AB_390913); Myc-tag 9B11 (Cell
590 Signaling Technology 2276; RRID:AB_331783); GM130 (BD Transduction Laboratories
591 610822; RRID:AB_398141); transferrin receptor (Clone MEM-189, MA1-19300,
592 ThermoFisher/Zymed; RRID:AB_2536952); and α-tubulin DM1A (Sigma-Aldrich T9026;
593 RRID:AB_477593). The following rabbit antibodies were used: HA-tag (Sigma-Aldrich H6908;
594 RRID:AB_260070); LAMP1 (Cell Signalling D2D11, monoclonal; RRID:AB_2687579); EEA1
595 (Cell Signalling Technology C45B10, monoclonal; RRID:AB_2096811); LIC1 (Cambridge
596 Bioscience HPA035013, polyclonal; RRID:AB_10600807); LIC2 (Abcam ab178702,
597 monoclonal); Nde1 (Proteintech, 10233-1-AP, polyclonal; RRID:AB_2149877). Secondary
598 antibodies: LI-COR IRDye secondary antibodies (800CW or 680RD: RRIDs AB_621846,
599 AB_621847, AB_621848, AB_2814912, AB_2716687); Alexa Fluor 488, Alexa Fluor 594,
600 Alexa Fluor 647, Cy3, or Cy5 labelled donkey anti-mouse, -rabbit and -sheep (Jackson
601 Immunoresearch, RRIDs AB_2340846, AB_2340854, AB_2340813, AB_2340819,
602 AB_2340862, AB_2313584, AB_2340621, AB_2340607, AB_2492288, AB_2307443,
603 AB_2340745 , AB_2340748, AB_2340751, AB_2340730).

604

605 **Constructs**

606 The following KASH5 constructs in pcDNA 4T/O have been previously described (Horn et al.,
607 2013): GFP-KASH5; GFP-KASH5ΔK; GFP-KASH5ΔNDΔK; GFP-KASH5ΔCDΔK; GFP-KASH5ND, as
608 has a myc-SUN2 construct in pcDNA3.1(-). EF-hand mutants were made using HiFi assembly
609 (New England Biolabs) by linearising GFP-KASH5 and GFP-KASH5ΔK using Q5 polymerase
610 with primers 5'GTCATGCGTGACTGGATTGCTG-3' and 5'-CGTGGAGTTGAGTATTTGCTCCTC-3'
611 and inserting synthetic G-block sequences (Integrated DNA Technologies) encoding KASH5
612 bps 97-319 with the appropriate mutations (see Fig. 8). HA-KASH5ΔK was made by
613 amplifying the KASH5ΔK sequence using forward primer 5'-
614 GCGCGGATCCGACCTGCCCGAGGGCCC-3' and reverse primer 5'-

615 GCGCGAATTCTTATGGATGTCGAGTGACTCTGAGC-3', digesting with BamH1 and EcoRI then
616 ligating into pcDNA3.1 containing the HA tag sequence. For generating a stable cell line, full
617 length GFP-KASH5 was inserted into the doxycycline-inducible lentiviral vector pTRIPZ (Open
618 Biosystem, Singapore) after amplification using primers 5'-
619 GCGCCTCGAGGACCTGCCCGAGGGCCCGGT-3' and 5'-
620 GCGCACGCGTTCACACTGGAGGGGGCTGGAGG-3' followed by digestion with XhoI and MluI.
621 Full length nesprin2α2 was amplified from a HeLa cDNA library and inserted into pcDNA3.1
622 downstream of GFP using XhoI and AflII digestion to give GFP-N2α2. A version lacking the
623 transmembrane and KASH domain was generated in the same vector to give GFP-N2α2ΔK.
624
625 Silently-mutated siRNA resistant full length hLIC1-mKate, hLIC2-mKate and hLIC2-GFP have
626 been previously described (Jones et al., 2014). RNAi-resistant full length LIC1 and LIC2 and
627 LIC1 truncations were generated by PCR and restriction digest cloning into pEGFP-C3
628 (Clontech) and used for rescue experiments. GFP-LIC1-CT2 encodes amino acids 1-456 of
629 human LIC1 with the addition of the amino acid sequence ADPPDLDN after the LIC1 C-
630 terminus. GFP-LIC1-CT3 encodes amino acids 1-387 followed by ADPPDLDN. N-terminally
631 Myc-tagged versions of full length human LIC1, LIC1-CT2 and LIC1-CT3 were generated using
632 the forward primer 5'-CAGCTGGTACCGCGGCCGTGGGGCGAGTC-3'. The reverse primers
633 were 5'-TCGAATCTAGACTAAGAAGCTTCTCCTTCCGTAGGAGATG-3' (full length LIC1), 5'-
634 TCGAATCTAGACTAAGAGCCAGTCTTTTTACTCAACAAAC-3' (LIC1-CT2) and
635 TCGAATCTAGACTATGGTGGTTGCTTTGCTAAAAGGGAC (LIC1-CT3), with no additional C-
636 terminal amino acids. PCR products were inserted into pcDNA-3.1 downstream of a myc-tag
637 sequence using KpnI and XbaI digestion. To generate LIC1 helix 1 mutants (FF: F447A, F448A
638 and AA: L451A, L452A), EGFP-LIC1 was linearised using Q5 polymerase (New England
639 Biolabs) with primers 5'-GTGTGAGTGGTGGTAGCCCTG-3' and 5'-
640 TGTAGCTCCAGCTTTCATGTTTGG-3'. A 111 bp single stranded ultramer (IDT) was used to
641 insert the appropriate mutated sequence using HiFi assembly (New England Biolabs). LIC1
642 helix 1 deletion mutants were generated in EGFP-LIC1 by Q5 amplification with
643 phosphorylated primers followed by blunt end ligation using the NEB Quick Ligation kit. The
644 primers for deletion or helix 1 (S440-T456) were 5'Phos-GGCTCTCCAGGAGGCCCTG and
645 5'Phos-TGTAGCTCCAGCTTTCATGTTTGGATC. For deletion of helix 1 and flanking sequences

646 (N433-S458) the primers were 5'Phos-CCAGGAGGCCCTGGTGTGAG-3' and 5'Phos-
647 TGGATCAATTTTTTTTGACCCAGCAGGAA-3'.
648
649 Vectors encoding mCherry-chicken p50 and RFP-CC1 have been previously described
650 (Wozniak et al., 2009). To generate GFP-BICD2N, the DNA sequence encoding amino acids 2-
651 402 of mouse BICD2 was amplified using forward primer, 5'-
652 GCGCGAATTCGTCGGCGCCGTCGGAGGAG-3'; reverse primer, 5'-
653 GCGCGGATCCTCACAGGCGCCGCAGGGCACT-3', then cloned into pEGFP-C1 (Clontech) using
654 EcoRI and BamHI. Other constructs were generous gifts from the following colleagues:
655 pMDG2.1-VSV-G and p8.91-Gag-Pol vectors (Apolonia et al., 2015; Zufferey et al., 1997), Dr
656 M. Malim (King's College London, UK); GFP-Rab11-FIP3 and GFP-Rab11-FIP3 I737E, (Wilson
657 et al., 2005), Prof. G. Gould (University of Glasgow, UK); pEGFP-C1 containing hRILP (Colucci
658 et al., 2005), Prof. Cecilia Bucci (University of Salento, Italy); pCB6-HA-RILP, Dr Mark Dodding
659 (University of Bristol, UK).
660
661 **Cell lines and transfection**
662 HeLa and hTERT-RPE cells were obtained from ATCC; Vero cells were purchased from
663 European Collection of Authenticated Cell Cultures. HeLaM cells were kindly provided by Dr
664 Andrew Peden, University of Sheffield, UK. Mycoplasma testing was routinely performed by
665 DAPI staining.
666
667 HeLa, HeLaM, HEK293T and Vero cells were maintained in DMEM supplemented with 10%
668 FBS at 8.0% CO_2 and 37°C. To generate cells stably expressing human GFP-KASH5, HeLa cells
669 were transfected with pTRIPZ-GFP-KASH5, pMDG2.1-VSV-G and p8.91-GAG-POL in a ratio of
670 4:1:2 to a total of 10 µg of DNA using Lipofectamine 2000 (ThermoFisher) as per the
671 manufacturer's instructions overnight. Virus was then collected and passed through a 0.45
672 µm filter before addition to cells for 4 hours. Transduced cells were selected for with fresh
673 media containing puromycin (3µg/ml). Induction of GFP-KASH5 expression was induced with
674 doxycycline (500ng/ml) for 16 hours. Transient transfection of HeLaM and Vero cells on #1.5
675 coverslips was achieved using JetPEI (PolyPlus transfection), using half the manufacturer's
676 recommended amounts of total DNA and JetPEI. Expression levels were carefully titrated for
677 each plasmid, in some cases using dilution with carrier DNA (pBluescript SK-II) (Flores-

678 Rodriguez et al., 2011), to avoid over-expression artefacts. For biochemical analysis, cells
679 were transfected in 10 cm dishes using either JetPEI, PEI (Sigma 408727) or FuGENE® HD
680 (E2311). PEI was dissolved at 1 mg/ml in 150 mM NaCl by incubation at 50°C, sterile filtered
681 and stored in aliquots at -80°C. Per dish, 16 µg of total DNA was diluted in 200 µl Opti-MEM
682 (Gibco 319850), 48 µl of PEI was added to another 200 µl of Opti-MEM, then after 5 min the
683 PEI was added to the DNA mix and incubated for 30 min at room temperature before adding
684 to the cells.
685
686 **Short interfering RNA (siRNA) methods**
687 For depletion of target genes, siRNA transfections used INTERFERin (PolyPlus Transfection).
688 siRNAs targeting the ORF of human LIC1 and LIC2 were obtained from Eurofins MWG
689 Operon. Oligonucleotides were applied to HeLaM cells at a final concentration of 5-20 nM
690 (for HeLaM) or 20 nM (for GFP-KASH5 HeLas) per target for 72 hours before analysis by
691 immunoblot and immunofluorescence. The following sequences were used, synthesised by
692 Eurofins MWG with dTdT overhangs: LIC1, 5'-AGAUGACAGUGUAGUUGUA-3'; LIC2, 5'-
693 ACCUCGACUUGUUGUAUAA-3' (Jones et al., 2014; Palmer et al., 2009); LIS1, 5'-
694 GAACAAGCGAUGCAUGAAG-3' (Lam et al., 2010; Tsai et al., 2005). For IC2, a SMARTpool
695 (Thermo Scientific Dharmacon) was used consisting of a mixture of four siRNAs: 5'-
696 GUAAAGCUUUGGACAACUA-3'; 5'-GAUGUUAUGUGGUCACCUA-3'; 5'-
697 GCAUUUCUGUGGAGGGUAA-3'; 5'-GUGGUUAGUUGUUUGGAUU-3'. Control RNAi
698 experiments were performed either using siGENOME lamin A/C Control (ThermoFisher
699 Scientific: Fig. 5 B-C, S3 A, B) or ON-TARGET-plus Non-targeting siRNA #1 (Thermo Scientific
700 Dharmacon). For transfection of siRNA-treated cells for biochemical or immunofluorescence
701 analysis, cells were depleted for 24 or 48 hrs then transfected with either JetPEI, PEI or
702 FuGENE® HD and incubated for a further 24 hr before lysate preparation or fixation. For LIC
703 rescue experiments, the LIC1 constructs used were siRNA-resistant (Jones et al., 2014).
704
705 **Immunoblotting**
706 For validating siRNA knock-down efficiency, lysates were collected 72 hours post siRNA
707 addition in RIPA lysis buffer (Sigma-Aldrich R0278) supplemented with cOmplete ULTRA
708 protease inhibitor (Roche 5892791001) and PhosSTOP (Roche PHOSS-RO) phosphatase
709 inhibitor. A total of 20 µg of protein was loaded per well diluted in denaturing SDS loading

710 buffer, and protein samples and molecular weight markers (PageRuler Plus Pre-stained
711 Protein Ladder, ThermoFisher Scientific 26619, or Colour pre-stained protein standards NEB
712 P7712 or P7719) were separated using 8%, 10% or 12% polyacrylamide gels before being
713 transferred to PVDF Immobilon-FL membrane with pore size 0.45 µm (Millipore Billerica,
714 MA, USA) using a Mini Trans-Blot electrophoretic transfer system (BioRad, Hertfordshire,
715 UK). The transfers were carried out in ice-cold transfer buffer at 100 V for 1.5 hours. After
716 transfer the membrane was blocked either by incubation in 5% dried milk (Marvel) in PBS
717 with 0.1 % Tween-20 (Sigma-Aldrich) (PBST) for 30 minutes at room temperature or in 1x
718 alpha-casein buffer (Sigma-Aldrich B6429) diluted in tris-buffered saline (TBS: 20 mM
719 Tris/HCl, pH 7.7, 150 mM NaCl) for 1 hour at room temperature. Primary antibodies were
720 diluted in 5% milk/PBST or 1x alpha-casein diluted in TBS supplemented with 0.01% Tween-
721 20 (TBST) and incubated at 4°C overnight. Membranes were washed three times in TBST or
722 PBST and incubated with LI-COR IRDye secondary antibodies (800CW or 680RD) diluted
723 1:10,000 in 5% milk/PBST or 1x alpha-casein in TBST for 1 hour at room temperature. Blots
724 were washed three times in PBST or TBST and once in water before imaging on a LI-COR
725 Odyssey or Odyssey CLx using Image Studio software.
726
727 **GFP-Trap immunoprecipitation**
728 For LIC1 truncation or mutant immunoprecipitation experiments, HeLa M cells were
729 depleted of endogenous LIC1 and LIC2 for 24 hours prior to transfection. Cells were
730 transiently transfected using PEI or JetPEI (see cell lines and transfection methods) and
731 incubated for 24 hours. Cells were washed with ice cold PBS and lysed in IP lysis buffer (50
732 mM Tris, pH 7.5, 10 mM NaCl, 2.5 mM $MgCl_2$, 1 mM DTT, 0.01% digitonin [Calbiochem
733 300410] and protease inhibitors, 10 µg/ml aprotinin [Sigma A6103], leupeptin [Calbiochem
734 108976] and pepstatin [Alfa Aesar J60237]) before centrifugation at 17,000 rpm for 30 mins
735 at 4°C in a microcentrifuge. For EGTA treatment, 1 mM EGTA was added to the lysis buffer
736 at this point. A tenth of the supernatant was taken as an input sample, and the remaining
737 supernatant was rotated at 4°C for 2 hours with ChromoTek GFP-Trap® magnetic agarose
738 beads pre-washed in IP wash buffer (50 mM Tris, pH 7.5, 10 mM NaCl, 1 mM DTT and
739 protease inhibitors). For EGTA treatment, 1 mM EGTA was added to the IP wash buffer.
740 Beads were isolated and washed three times in IP wash buffer and proteins eluted by
741 boiling at 95°C in SDS-PAGE sample buffer before analysis by SDS-PAGE and

742 immunoblotting. For LIC mutant immunoprecipitations, cells were transfected using
743 FuGENE® HD transfection reagent, as per manufacturer's instructions, with a reagent:DNA
744 ratio of 3:1 and incubated for a further 24 hours following endogenous LIC depletion. The
745 buffers contained 50 mM NaCl, and 0.01% digitonin was added to the wash buffer.
746
747 **BAPTA-AM treatment**
748 HeLaM cells were grown on uncoated #1.5 glass coverslips and Vero cells were grown on
749 coverslips coated with 1µg/ml Fibronectin (Sigma F0895) then transfected. Cells were
750 treated with either 10 µM BAPTA-AM (Abcam ab120503) or DMSO vehicle control for 2
751 hours before fixation and immunofluorescence labelling.
752
753 **Quantification of immunoblots**
754 Protein band signal intensity was measured using LI-COR Image Studio Lite software or
755 ImageJ, and blot background signal intensity was subtracted. For siRNA knock-down
756 experiments, band signal intensity was normalised to total protein. Protein amount was
757 then expressed as a percentage compared to control siRNA samples, which were set as
758 100%. For immunoprecipitation experiments, the enrichment factor for GFP or each GFP-
759 tagged protein in the pull-down was first calculated as bound/input=*x*. For each prey,
760 bound/input=*y* was calculated, and then the efficiency of pull-down compared to GFP was
761 determined as a percentage (*y*/*x**100). For GFP-trap pull-downs from siRNA-treated cells,
762 the prey protein levels could not be normalised compared to input levels if that protein had
763 been depleted. Instead, the amount of each prey protein in the control-depleted GFP-
764 KASH5DK pull-downs was set as 100%, and the amount present in other samples was
765 compared to that.
766
767 **Immunofluorescence**
768 HeLaM or Vero cells were grown on #1.5 coverslips at appropriate density. For EEA1
769 antibody labelling cells were fixed for 20 mins in 3% formaldehyde in PBS at RT. After
770 washing, unreacted formaldehyde was quenched with glycine (0.1 M) and permeabilised in
771 0.1% Triton X-100 in PBS for 10 mins before PBS wash prior to antibody labelling. For all
772 other antibody labelling, cells were fixed in methanol for 10 minutes at -20˚C and washed in
773 PBS. Secondary antibodies labelled with Alexa Fluor 488, Alexa Fluor 594, Alexa Fluor 647,

774 Cy3, or Cy5 were used along with 1 µg/ml DAPI, and samples were mounted in ProLong Gold
775 (Invitrogen). For LIS1 antibody labelling (Baffet et al., 2015), coverslips were washed once in
776 PBS then incubated for 1 min in PHEM buffer (60 mM PIPES, 25 mM HEPES, 10 mM EGTA,
777 2mM $MgCl_2$, pH 6.9) containing 0.5% Triton X-100. Cells were then transferred to PHEM
778 buffer supplemented with 3.7% paraformaldehyde for 20 minutes. This was followed by
779 incubation in 0.2% Triton X-100 in PBS for 5 minutes. Coverslips were rinsed in PBS and
780 quenched with glycine before labelling.
781
782 **Imaging and analysis**
783 Fixed HeLaM (Fig. 4 D; 5 D&E; 6 B, C; 8 C; S3 C, D; S4 E and S5A) and Vero cells (Fig. S5 B)
784 were imaged using an Olympus BX60 or BX50 microscope (Olympus Keymed) with a Plan
785 apochromat 60X 1.4 N.A. oil immersion objective, CoolLED light source (CoolLED Ltd) or
786 100W Hg lamp, CoolSNAP ES CCD camera (Teledyne Photometrics) and MetaVue software
787 (Molecular Devices). Subsequent image analysis was performed using MetaVue and ImageJ
788 software. The imaging in Fig. 1-3, 5 A, 6 A and S3 A was performed on a IX71 microscope
789 (Olympus) which was equipped for optical sectioning by a DeltaVision CORE system (GE
790 Healthcare) with z-spacing fixed at 0.2 µm. Plan Apochromat 60X 1.4 N.A. or UPlanFl 100X
791 1.35 N.A. oil immersion objective lenses (Olympus) were used with a CoolSNAP HQ CCD
792 camera (Photometrics). Deconvolution was completed using SoftWorX (Applied Precision)
793 and images are displayed as z-projections.
794
795 Line scans were generated using Image J using the plot profile tool, with the lines starting in
796 the cytoplasm. Data was exported and plotted as graphs in GraphPad Prism. ImageJ was
797 used to generate inverted greyscale images, merge channels, and draw cell outlines, using
798 contrast-adjusted images as a guide, where needed. Some images were prepared and
799 annotated using Adobe Photoshop. For phenotype scoring, each experiment was performed
800 at least three times, and the number of cells manually scored are given in the Figure
801 legends. Examples of the Golgi apparatus, early endosome and lysosome phenotypes are
802 shown in Figs 5 and S3. For dynein recruitment to KASH5 in Fig. 3 D, 4 E, 8 C and Fig. S1 C
803 and D, cells were scored in a binary fashion as to whether dynein or dynactin could be seen
804 at the NE. For the analysis shown in Figs. 4 and 8, the scoring was performed without
805 knowing the sample identity. Cells with strong nuclear enrichment of GFP-KASH5 and HA-

806 SUN1 (Fig. 8) or GFP-KASH5 and myc-SUN2 (Fig. 4), but with limited accumulation in the ER,
807 were selected without reference to the LIC1 channel, which was then used to score for
808 dynein recruitment. For these data, statistical tests were not deemed appropriate as there
809 was no variation in some control conditions, with all cells recruiting dynein or dynactin to
810 KASH5. For other datasets, the statistical tests used are given in the figure legends. For
811 experiments where one condition was compared to a control, an unpaired t-test was
812 performed using GraphPad Prism (GraphPad Software). For multiple comparisons, one-way
813 ANOVA was used if all data points were present. In Fig. 4E, ANOVA could not be used
814 because four data points were missing (out of a possible 49). Instead, a mixed model was
815 implemented using Prism, fitted using Restricted Maximum Likelihood (REML) with Geisser-
816 Greenhouse correction. Tukey's multiple comparison was used for ANOVA and REML
817 analysis. For experiments where categoric phenotype scoring data across multiple
818 conditions were compared to one control, multinomial logistic regression was applied using
819 SPSS (IBM) software (Lam et al., 2010). Full statistical analysis is given in Supplementary
820 tables 2-4. Graph preparation was performed in Prism. Figures were assembled using Adobe
821 Illustrator (Adobe) or Affinity Designer (Serif Europe Ltd).
822
823 **Recombinant KASH5 protein expression and purification**
824 Constructs of human KASH5 (amino acid residues: 1-115, 155-349, 1-349, 1-407, 1-460 and
825 1-507) were cloned into pMAT11 vector (Peranen et al., 1996) for expression with an N-
826 terminal TEV-cleavable His_6-MBP tag. KASH5 constructs were expressed in BL21 (DE3) cells
827 (Novagen), in 2xYT media, and induced with 0.5 mM IPTG for 16 hr at 25°C. Bacterial pellets
828 were harvested, resuspended in 20mM Tris pH 8.0, 500 mM KCl and lysed using a TS Cell
829 Disruptor (Constant Systems) at 172 MPa. Cellular debris were later removed by
830 centrifugation at 40,000 g. KASH5 fusion proteins were purified through consecutive Ni-NTA
831 (Qiagen), amylose (NEB), and HiTrap Q HP (Cytiva) ion exchange chromatography. The N-
832 terminal His_6-MBP tag was cleaved using TEV protease and the cleaved samples were
833 further purified through HiTrap Q HP (Cytiva) ion exchange chromatography and size
834 exclusion chromatography (HiLoad 16/600 Superdex 200, Cytiva) in 20 mM HEPES pH 7.5,
835 150 mM KCl, 2 mM DTT. Purified KASH5 protein samples were spin concentrated using
836 Amicon® Ultra centrifugal filter device (10,000 NMWL), flash-frozen in liquid nitrogen and
837 stored at -80°C. Purified KASH5 proteins were analysed using SDS-PAGE and visualised with

838 Coomassie staining. Protein concentrations were determined using Cary 60 UV
839 spectrophotometer (Agilent) with extinction coefficients and molecular weights calculated
840 by ProtParam (http://web.expasy.org/protparam/).
841
842 **Multi-angle light scattering coupled with size exclusion chromatography (SEC-MALS)**
843 The absolute molar masses of KASH5 protein samples were determined by multi-angle light
844 scattering coupled with size exclusion chromatography (SEC-MALS). KASH5 protein samples
845 at > 1.5 mg ml^{-1} were loaded onto a Superdex™ 200 Increase 10/300 GL size exclusion
846 chromatography column (Cytiva) in 20 mM Tris pH 8.0, 150 mM KCl, 2 mM DTT, at
847 0.5 ml min^{-1}, in line with a DAWN® HELEOS™ II MALS detector (Wyatt Technology) and an
848 Optilab® T-rEX™ differential refractometer (Wyatt Technology). Differential refractive index
849 and light scattering data were collected and analysed using ASTRA® 6 software (Wyatt
850 Technology). Molecular weights and estimated errors were calculated across eluted peaks
851 by extrapolation from Zimm plots using a dn/dc value of 0.1850 ml g^{-1}. Bovine serum
852 albumin (ThermoFisher) was used as the calibration standard.
853
854 **Protein purification**
855 Human LIS1 (Baumbach et al., 2017) and full length wild type human cytoplasmic dynein-1
856 (Schlager et al., 2014a), or a version containing heavy chain phi-disrupting mutations
857 R1567E and K1610E that prevent the phi autoinhibitory conformation of dynein (Zhang et
858 al., 2017), were expressed using the *Sf*9/baculovirus system and purified as previously
859 described (Baumbach et al., 2017; Schlager et al., 2014a). Pellets from 1 L of Sf9 cell culture
860 were suspended in 50 ml lysis buffer (50 mM HEPES pH 7.2, 100 mM NaCl, 1 mM DTT, 0.1
861 mM Mg.ATP, 10% Glycerol), supplemented with one cOmplete tablet (Roche) and 1mM
862 PMSF. Cells were lysed using a Dounce homogeniser at 4°C, then lysate clarified for 45 mins
863 at 500,000 x *g*. The supernatant was incubated with 1.5 ml pre-equilibrated IgG beads
864 (Cytiva) for 3 h. Beads were washed with 200 ml lysis buffer. For dynein, beads were then
865 transferred to a 2 ml tube, adding 10 µM SNAP-Cell TMR-Star dye (New England Biolabs)
866 and incubating for 1 h at 4°C. Beads for both constructs were then washed with 100 ml TEV
867 buffer (50 mM Tris-HCl pH 7.4, 148 mM K-acetate, 2 mM Mg-acetate, 1 mM EGTA, 10%
868 Glycerol, 0.1 mM Mg.ATP, 1 mM DTT), then transferred again to a 2 ml tube, adding 400 µg
869 TEV protease and incubating overnight at 4°C. Sample was then concentrated and gel

870 filtered using a $G4000_{SWXL}$ 7.8/300 column (TOSOH Bioscience) into GF150 buffer (25 mM
871 HEPES pH 7.2, 150 mM KCl, 1 mM $MgCl_2$, 5 mM DTT, 0.1 mM Mg.ATP) for dynein, or TEV
872 buffer for Lis1. Peak fractions were concentrated and snap-frozen in liquid nitrogen.
873
874 Dynactin was purified from frozen porcine brains as previously described (Urnavicius et al.,
875 2015). Porcine brains were blended with 300 ml homogenisation buffer (35 mM PIPES pH
876 7.2, 5 mM $MgSO_4$, 1 M KCl, 200 µM EGTA, 100 µM EDTA, 1 mM DTT) supplemented with
877 four cOmplete tablets and 1mM PMSF until just thawed. The lysate was then clarified in two
878 steps: 15 mins at 38,400 x *g* at 4°C, then 50 mins at 235,000 x *g* at 4°C. All subsequent steps
879 were carried out at 4°C The supernatant was then filtered through a GF filter then a 0.45 µm
880 filter, then loaded onto an SP Sepharose column (Cytiva), equilibrated with SP buffer A (35
881 mM PIPES pH 7.2, 5 mM $MgSO_4$, 1 mM EGTA, 0.5 mM EDTA, 1 mM DTT, 0.1 mM Mg.ATP).
882 The resin was then washed until white using 99.5% SP buffer A/0.5% SP buffer B (35 mM
883 PIPES pH 7.2, 5 mM $MgSO_4$, 1 M KCl, 1 mM EGTA, 0.5 mM EDTA, 1 mM DTT, 0.1 mM
884 Mg.ATP), then dynactin was eluted using a gradient from 0.5-25% (% SP buffer B). Dynactin-
885 containing fractions were then filtered through a 0.22 µm filter, then loaded onto a Mono Q
886 HR 16/60 column (Cytiva), pre-equilibrated with Mono Q buffer A (35 mM PIPES pH 7.2, 5
887 mM $MgSO_4$, 200 µM EGTA, 100 µM EDTA, 1 mM DTT). This column was washed with 10 CV
888 Mono Q buffer A, then dynactin eluted using a 15-35% gradient (% Mono Q buffer B, 35 mM
889 PIPES pH 7.2, 5 mM $MgSO_4$, 1 M KCl, 200 µM EGTA, 100 µM EDTA, 1 mM DTT). Peak
890 fractions were concentrated and gel filtered using a $G4000_{SW}$ 21.5/600 column (TOSOH
891 Bioscience) into GF150 buffer, with the peak concentrated and snap-frozen in liquid
892 nitrogen.
893
894 Strep-tagged human Hook3 (1-522) (Urnavicius et al., 2018) was purified using the
895 *Sf*9/baculovirus system as previously described (Urnavicius et al., 2018). A pellet from 500
896 ml of Sf9 culture was thawed using 50 ml Strep-tag lysis buffer (30 mM HEPES pH 7.2, 50
897 mM K-Acetate, 2 mM Mg-Acetate, 1 mM EGTA, 10% Glycerol, 1 mM DTT) plus one
898 cOmplete tablet and 1 mM PMSF. Cells were then lysed using a Dounce homogeniser, with
899 the lysate clarified for 20 minutes at 50,000 x *g* at 4°C. Supernatant was filtered using a GF
900 filter, then flown onto a StrepTrap HP 1 ml column (Cytiva) at 4°C, washed using 40 CV
901 Strep-tag lysis buffer, then eluted with 3 mM desthiobiotin. Peak fractions were

902 concentrated and gel filtered using a Superose 6 10/300 Increase column (Cytiva) into
903 GF150 buffer. The monodisperse peak was concentrated and snap-frozen in liquid nitrogen.
904
905 ***in vitro* TIRF motility assays**
906 *in vitro* TIRF assays were carried out as previously (Urnavicius et al., 2018). Microtubules
907 were typically prepared the day before the assay. Microtubules were made by mixing 1 µl of
908 HiLyte Fluor 488 tubulin (2 mg/ml, Cytoskeleton), 2 µl biotinylated tubulin (2 mg/ml,
909 Cytoskeleton) and 7 µl unlabelled pig tubulin (Schlager et al., 2014a) (6 mg/ml) in BRB80
910 buffer (80 mM PIPES pH 6.8, 1 mM $MgCl_2$, 1 mM EGTA, 1 mM DTT). 10 µl of polymerization
911 buffer (2× BRB80 buffer, 20% (v/v) DMSO, 2 mM Mg.GTP) was added, then the solution was
912 incubated at 37°C for 1 h for microtubule polymerization. The sample was diluted with 100
913 µl of MT buffer (BRB80 supplemented with 40 µM paclitaxel), then centrifuged at 21,000 x *g*
914 for 9 minutes at room temperature to remove soluble tubulin. The resulting pellet was
915 gently resuspended in 100 µl of MT buffer, then centrifuged again as above. 50 µl MT buffer
916 was then added, with the microtubule solution then stored in a light-proof container. Before
917 usage, and every 5 hours during data collection, the microtubule solution was spun again at
918 21,000 x *g* for 9 minutes, with the pellet resuspended in the equivalent amount of MT
919 buffer.
920
921 Assay chambers were prepared by applying two strips of double-sided tape on a glass slide,
922 creating a channel, then placing a piranha-solution-cleaned coverslip on top. The coverslip
923 was then functionalized using PLL-PEG-Biotin (SuSOS), washed with 50 µl of TIRF buffer (30
924 mM HEPES pH 7.2, 5 $MgSO_4$, 1 mM EGTA, 2 mM DTT), then incubated with streptavidin (1
925 mg/ml, New England Biolabs). The chamber was again washed with TIRF buffer, then
926 incubated with 10 µl of a fresh dilution of microtubules (2 µl of microtubules diluted into 10
927 µl TIRF-Casein buffer (TIRF buffer supplemented with 50 mM KCl and 1 mg/ml casein)) for 1
928 min. Chambers were then blocked with 50 µl blocking buffer.
929
930 Complexes were prepared mixing 1.5 µl of each component at the following concentrations:
931 dynein at 0.3 µM, dynactin at 0.3 µM, adaptor at 6 µM, Lis1 at 50 µM. GF150 buffer was
932 added to a final volume of 6 µl. Complexes were incubated on ice for 15 minutes then
933 diluted with TIRF-Casein buffer to a final buffer of 15 µl. Four microliters of complex were

934 added to 16 µl of TIRF-Casein buffer supplemented with an oxygen scavenging system (0.2
935 mg/ml catalase, Merck; 1.5 mg/ml glucose oxidase, Merck; 0.45% (w/v) glucose) 1% BME, 5
936 mM Mg.ATP. This mix was flowed into the chamber.
937
938 The sample was imaged immediately at 23°C using a TIRF microscope (Nikon Eclipse Ti
939 inverted microscope equipped with a Nikon 100x TIRF oil immersion objective). For each
940 sample, a microtubule image was acquired using a 488 nm laser. Following this a 500-frame
941 movie acquired (200 ms exposure, 4.1 fps) using a 561 nm laser. To analyse the data, ImageJ
942 was used to generate kymographs from the tiff movie stacks. These kymographs were
943 blinded, then events of similar length were picked to analyse velocity and number of
944 processive events/µm microtubule/s, using criteria outlined previously (Schlager et al.,
945 2014a; Urnavicius et al., 2018). Velocity was calculated using pixel size of 105 nm and frame
946 rate of 235 ms/frame. Three replicates were taken for each sample, with velocities and
947 number of processive events plotted using GraphPad Prism 7, using ANOVA with Tukey's
948 multiple comparison to test significance.
949
950 **Supplementary material**
951 Fig. S1. illustrates the meiotic LINC complex, dynein, dynactin, and the role of dynein in
952 meiotic prophase I. It also demonstrates the effect of IC2 and LIS1 depletion on dynein and
953 dynactin recruitment to KASH5. Fig. S2 shows immunoblot analysis demonstrating depletion
954 of targets by RNAi. Fig. S3 shows that LICs 1 and 2 act redundantly in endocytic organelle
955 positioning, with helix 1 being essential. Fig. S4 demonstrates that LICs act redundantly to
956 recruit dynein and dynactin to RILP-positive late endosomes, and that dynein recruitment
957 requires helix 1. Fig. S5 depicts the effect of BAPTA-AM treatment on dynein recruitment to
958 KASH5 and Rab11-FIP3, and that KASH5-dynein interactions are not affected by EGTA in
959 vitro. Table S1 contains the quantitation of blots from Figs. 1 C and 3 E. Tables S2-4
960 document the full multinomial logistic regression analysis of the data shown in Figs. 5 C, 8 E,
961 S3 C and D.
962
963 **Acknowledgements**
964 The work in V. Allan's laboratory was funded by the Biotechnology and Biological Sciences
965 Research Council (BB/N006933/1 and a Ph.D. studentship to E. Granger), the Medical

966 Research Council (Ph.D. studentship to C. Villemant), and the University of Manchester. A.
967 Salter was funded by the University of Manchester-A*STAR Research Attachment
968 Programme (ARAP). We thank Quentin Roebuck and Peter Stanley for excellent technical
969 assistance. The Bioimaging Facility microscopes used in this study were purchased with
970 grants from BBSRC, Wellcome and the University of Manchester Strategic Fund. We would
971 like to thank Drs Peter March and Graham Wright for their help with microscopy in
972 Manchester and Singapore, respectively. The work in B. Burke's laboratory was funded by
973 the Singapore Biomedical Research Council and the Singapore Agency for Science
974 Technology and Research, A*STAR. We are grateful to Dr Alessandra Calvi for generating the
975 nesprin2α construct. O. Davies is funded by a Wellcome Senior Research Fellowship (Grant
976 Number 219413/Z/19/Z). C. Lau was funded by grants from the Wellcome Trust (WT210711)
977 and the Medical Research Council, UK (MC_UP_A025_1011), awarded to Dr Andrew Carter.
978 For the purpose of open access, the author has applied a CC BY public copyright licence to
979 any Author Accepted Manuscript version arising from this submission.
980
981 The authors declare no competing financial interests.
982
983 **Author contributions**
984 Conceptualization: V. Allan, B. Burke. Funding acquisition: V. Allan, B. Burke. Designed,
985 performed experiments, and analysed data: A. Salter, K. Garner, V. Allan, C. Villemant, E.
986 Granger, M. Gurusaran, C. Lau, O. Davies. Generated molecular reagents: G. McNee, C.
987 Villement, A. Salter, V. Allan, E. Granger, K. Garner. Purified proteins: C. Lau, M. Gurusaran.
988 Supervision: V. Allan, B. Burke, P. Woodman, O. Davies. Visualization/data presentation: A.
989 Salter, K. Garner, V. Allan, C. Villemant, E. Granger, M. Gurusaran, C. Lau. Writing the initial
990 draft: A. Salter, K. Garner, V. Allan, C. Lau. Review & editing: all authors.
991

992 **Figure legends**

993

994 **Figure 1. Recruitment of dynein, dynactin and LIS1 to KASH5 in HeLa cells.**

995 **(A)** A stable HeLa cell line inducibly expressing GFP-KASH5 (green) was labelled with
996 antibodies against dynein IC and LIC1, dynactin p150 and p50, LIS1 and Nde1 (magenta) and
997 imaged on a DeltaVision microscope. Images are z-projections of deconvolved image stacks.
998 The bottom panel shows the transient expression of GFP-N2α2 in green and labelling with
999 anti-LIC1 in magenta, with undeconvolved wide-field images. Arrowheads point out the
1000 location of centrosomes, full arrows show creases in the NE and asterisks mark cytoplasmic
1001 accumulations of GFP-KASH5. Thin white lines on colour merge images show where a line
1002 scan plot was performed, shown on the right. Scale bars = 10 µm. **(B)** Schematic showing
1003 KASH5 and the constructs used. For some experiments, the GFP was replaced with an HA
1004 tag. **(C)** Dynein, dynactin and LIS1 are recruited to KASH5 as shown by GFP-Trap pull-downs.
1005 HeLaM cells were transiently transfected with GFP-KASH5ΔK or GFP-N2α2ΔK. The pull-
1006 downs and inputs (1.5% of total lysate) were probed with antibodies against GFP, p150, IC,
1007 LIC1, LIC2, LIS1, BICD2 and α-tubulin. Molecular weight markers are shown. Quantitation of
1008 the blot is given in Table S1. **(D)** The KASH5 N-terminal EF-hand domain is sufficient to
1009 recruit dynein. Lysates of HeLaM cells expressing GFP, GFP-KASH5ΔK (GFP-K5ΔK) or GFP-
1010 KASH5 N terminus (GFP-K5ND) were isolated by GFP-trap and probed for LIC1 by
1011 immunoblotting. The input is 15% of the GFP-trap sample. The graph shows quantitation of
1012 LIC1 levels in pull-downs (n=3 independent experiments), normalised to GFP-K5ND.

1013

1014 **Figure 2. Dynein and LIS1 recruitment to KASH5 does not require interaction between**
1015 **dynein IC and dynactin p150**.

1016 **(A)** HeLa cells stably expressing GFP-KASH5 (green) were depleted of IC2 using 20 nM siRNA
1017 for 72 hours and then processed for immunofluorescence with antibodies against LIC1,
1018 dynactin p150 and LIS1 (magenta). White lines on colour merge images show where a line
1019 scan plot was performed, shown on the right. **(B)** HeLa cells were transiently transfected
1020 with GFP-KASH5, RFP-CC1 and myc-SUN2 (CC1 and SUN2: not shown. Cells expressing CC1
1021 are marked with asterisks). Cells were fixed and labelled with antibodies against dynein IC
1022 and LIC1, dynactin p50 and p150, and LIS1. Green lines on the GFP-KASH5 images indicate

1023 line scan locations, shown on the right. Images were taken on a DeltaVision microscope and
1024 z-stack projections of deconvolved images are shown. Scale bars = 10 µm.
1025
1026 **Figure 3. Dynein is recruited to KASH5 via either LIC1 or 2.**
1027 **(A-D)** HeLa cells stably expressing GFP-KASH5 (green) were depleted of LIC1 **(A)**, LIC2 **(B)**, or
1028 both LIC1 and 2 **(C)** using 10 nM of each siRNA for 72 hours, then fixed and labelled with
1029 antibodies against IC, dynactin p150 or LIS1 (magenta). Thin white lines show where a line
1030 scan plot was performed on LIC1&2 depleted cells, shown on the right. Images were taken
1031 on a DeltaVision microscope and z-stack projections of deconvolved images are shown.
1032 Scale bars = 10 µm. **(D)** LIC depleted cells were scored in a binary fashion for recruitment of
1033 IC, p150 or LIS1 to KASH5. The mean and standard deviation of each condition is shown. The
1034 experiment was repeated three times, with 300 cells scored for each condition in each
1035 experiment. **(E)** HeLaM cells were depleted with siRNA against both LICs together (10 nM
1036 each), or with control siRNAs. 48 hours into the knockdown, cells were transfected with
1037 either GFP-KASH5ΔK or GFP-N2α2ΔK. The following day cells were lysed and a GFP trap was
1038 performed. Input and pull-downs were immunoblotted with antibodies against GFP, p150,
1039 LIC1, LIC2, IC and α-tubulin. The input was 1.5% of the total cell lysate. Molecular weight
1040 markers are shown on the right. Quantitation of the blot is given in Table S1.
1041
1042 **Figure 4. KASH5-LIC1 interactions require LIC1 helix 1.**
1043 **(A)** Schematic of LIC1 showing the GTPase-like domain that is highly conserved between
1044 LICs, and a less well conserved C terminal domain containing helix 1 (440-456) and helix 2
1045 (493-502). The constructs used are: truncations lacking helix 2 (LIC1 CT2) or both helix 1 and
1046 helix 2 (LIC1 CT3); point mutations within Helix 1 (FF: F447A/F448A and LL: L451A/L452A);
1047 helix 1 deletions (Δ440-456 and Δ433-458). **(B, C)** HeLaM cells were depleted of both LICs by
1048 siRNAs for 48 hours, then co-transfected and incubated for a further 24 hours with Myc-
1049 tagged LIC1 constructs and GFP-KASH5ND or GFP as a control (B) or GFP-LIC1 constructs and
1050 HA-KASH5ΔK (C). Cell lysates were incubated with GFP-trap beads then analysed by SDS-
1051 PAGE and immunoblotting with antibodies to GFP, myc and IC (IC74) to detect native
1052 dynein, as indicated. The input is 15% of the GFP-trap sample. Quantitation of myc-LIC1 pull-
1053 down efficiency (B) with GFP-KASH5ND vs. myc-LIC1-FL was 177% for LIC1-CT2 and 8.0% for
1054 LIC1-CT3 (n=2). Quantitation of HA-KASH5DK pull-down efficiency (C) vs. GFP-LIC1-WT was

1055 3.9±3% for LIC1-FF, 3.3±4.9% for LIC1Δ433-458 and 1.9±2.1% for LIC1Δ440-456 (±S.D., n=3)
1056 and 3.1% for LIC1-LL (n=2). **(D, E)** HeLaM cells were co-transfected with GFP-tagged LIC1
1057 constructs, HA-KASH5 and myc-SUN2 for ~18 hours, then fixed and labelled with antibodies
1058 to HA, GFP and myc (not shown) and imaged by wide-field microscopy. Cells with strong
1059 enrichment of KASH5 and SUN2 at the NE were scored for the presence or absence of GFP
1060 at the NE without knowing the identity of the LIC1 construct expressed (see methods). **(D)**
1061 Example wide-field images with line scans (black lines on the images): GFP-LIC1 constructs
1062 shown in green, HA-KASH5 in black. GFP-LIC1-WT is recruited to HA-KASH5 (top panels)
1063 whereas GFP-LIC1-CT3 is not (bottom panels). Scale bar = 10 µm. **(E)** Recruitment of GFP-
1064 LIC1 proteins to the NE was scored in a binary fashion from 5-7 experiments with 25-82 cells
1065 scored per experiment per construct. The total number of cells scored for each condition is
1066 shown above the line. A mixed effects analysis was performed (see methods) with Tukey's
1067 multiple comparison test to compare GFP-LIC1 FL recruitment vs. all others (P≤0.0001=****,
1068 ≤0.001=***, ≤0.01=**). No other comparisons gave significant P-values.
1069
1070 **Figure 5. LICs 1 and 2 act redundantly in Golgi apparatus positioning, with helix 1 being**
1071 **essential.**
1072 **(A-C)** HeLaM cells were depleted of LIC1, LIC2 or both LICs using 5 nM siRNA for each
1073 subunit, then analysed by immunoblotting of lysates with antibodies to LIC1 and 2 **(A)**, or
1074 fixed and labelled with antibodies to GM130 and imaged on a DeltaVision microscope to
1075 reveal the Golgi apparatus **(B)**. Z-projections of deconvolved images stacks are shown.
1076 Quantitation of knock-down efficiency is shown in Fig. S2C. **(C)** Golgi morphology was scored
1077 manually for 100 cells per condition, in 3 independent experiments. Mean ±SD values are
1078 plotted. Statistical analysis was performed using multinomial logistic regression (see Table
1079 S2 for full results): comparisons vs. control samples are shown on the graph
1080 (P≤0.0001=****). **(D, E)** HeLaM cells were depleted of both LICs then transfected with RNAi-
1081 resistant LIC1-mKate or LIC2-mKate **(D)** or GFP-LIC1-FL, GFP-LIC1-CT2, GFP-LIC1-CT3 and GFP
1082 constructs **(E)**. Cells treated with control siRNAs and transfected with GFP were used as
1083 controls. GM130 labelling was used to reveal Golgi apparatus morphology (wide-field
1084 images: asterisks mark cells expressing the constructs). Golgi morphology was scored for
1085 ~100 cells per experimental condition in three independent experiments **(E)**. Mean ±SD
1086 values are plotted. GFP and GFP-LIC1-CT3 rescue data are significantly different to control

1087 knockdown (P≤0.0001), whereas rescue with GFP-LIC1-FL or GFP-LIC1-CT2 are not
1088 (multinomial logistic regression, see table S2). All scale bars = 10 µm.
1089
1090 **Figure 6. KASH5 has properties of a dynein adaptor.**
1091 **(A)** HeLaM cells transiently expressing GFP-KASH5ΔK or GFP-KASH5ΔNΔK (which lacks the
1092 dynein binding domain) were labelled with GM130 or LAMP1 antibodies (z-stack projections
1093 of deconvolved images shown). Cells were scored for phenotypes associated with dynein
1094 inhibition: Golgi apparatus scattering, peripheral clustering of lysosomes and enlarged
1095 lysosomes. Manual scoring of 100 cells per condition was repeated in three independent
1096 experiments, with mean and S.D. shown. An unpaired t-test was performed comparing GFP-
1097 KASH5ΔK- and GFP-KASH5ΔNΔK-expressing cells for each phenotype. **** = p≤0.0001, ***
1098 = p≤0.001, ** = p≤0.01. **(B, C)** Full length HA-KASH5 **(B)** or HA-RILP **(C)** were expressed alone
1099 (top panel, control) or with dominant negative GFP-BICD2N (middle panel), or dominant
1100 negative GFP-Rab11-FIP3-I73E (bottom panel) in HeLaM cells. Endogenous dynein was
1101 visualised along with HA-KASH5 or HA-RILP using antibodies to LIC1 and HA (wide-field
1102 imaging, scale bar = 10 µm). Thin black and white (left panels) or red lines (LIC1 panels)
1103 show where line scan plots were performed (right).
1104
1105 **Figure 7. KASH5 is an activating adaptor for dynein motility in vitro.**
1106 **(A)** SDS-PAGE and Coomassie blue staining of purified bacterially-expressed KASH5
1107 truncations. KASH5$_{1-115}$ contains the EF hands; KASH5$_{155-349}$ consists of only the coiled coil;
1108 KASH5$_{1-349}$ is the EF hand plus coiled coil; KASH5$_{1-407}$, KASH5$_{1-460}$ and KASH5$_{1-507}$ all contain
1109 the EF hands, coiled coil, and additional sequence. **(B)** SEC-MALS analysis of purified KASH5
1110 truncations, showing the measured M_w. The predicted dimeric M_w values are: KASH5$_{1-407}$, 92
1111 kDa; KASH5$_{1-460}$, 103 kDa; KASH5$_{1-507}$, 114 kDa. **(C)** Purified baculovirus-expressed
1112 recombinant dynein containing a heavy chain R1567E/K1610E mutant that cannot form the
1113 inhibited Phi conformation, LIS1 and porcine brain dynactin were combined with KASH5$_{1-407}$,
1114 KASH5$_{1-460}$ or KASH5$_{1-507}$ and motility of individual 6-carboxytetramethylrhodamine-labelled
1115 dynein molecules along microtubules was visualised using TIRF microscopy and displayed as
1116 kymographs. **(D)** Motility of wild-type recombinant dynein, LIS1 and dynactin in the
1117 presence or absence of KASH5$_{1-460}$, with the activating adaptor Hook3$_{1-522}$ as a positive
1118 control. **(E)** Analysis of motility from (D). Left panel: the number of processive events per µm

1119 microtubule per minute from was determined from kymographs in a blinded fashion for all
1120 three conditions in three technical replicates, with the mean ± S.D. plotted. The total
1121 number of movements analysed were 2066 for Hook3, 339 for KASH5 and 34 for the no
1122 addition control. Significance was determined using ANOVA with Tukey's multiple
1123 comparison (ns = not significant, * = p≤0.05, **** = p≤0.0001). Right panel: the mean
1124 velocity of processive dynein movements from the $KASH5_{1-406}$ and $Hook3_{1-522}$ data are
1125 plotted (± S.D., n=3 replicates). **(F)** Kymographs of 6-carboxytetramethylrhodamine-labelled
1126 wild-type dynein molecules combined with LIS1, dynactin and $KASH5_{1-115}$, $KASH5_{155-349}$, or
1127 $KASH5_{1-349}$.
1128
1129 **Figure 8. KASH5's EF hand is critical for dynein and dynactin complex assembly.**
1130 **(A**) Top: Sequence comparison between human KASH5 and other dynein adaptors
1131 containing EF-hands, and between KASH5 proteins from different species. The EF-hand
1132 consensus sequence is shown, along with position nomenclature (Grabarek, 2006). Bottom:
1133 mutations generated in KASH5 EF-hands (altered amino acids shown in red), along with
1134 published mutations in the calcium-dependent dynein adaptor CRACR2a (Wang et al., 2019).
1135 Summary of KASH5 mutant dynein-binding activity, as indicated by + or - symbols. **(B)** GFP-
1136 trap immunoprecipitates from cells expressing GFP-hKASH5ΔK, GFP-hKASH5ΔK EF hand
1137 mutants, or GFP, probed with antibodies to GFP, dynein IC and dynactin p150. Quantitation
1138 of IC and p150 levels normalised to GFP-LIC1-WT levels (n=3 experiments) is plotted
1139 graphically below. **(C, D)** HeLaM cells were transiently transfected with GFP-KASH5-WT or EF
1140 hand mutants along with HA-SUN1 (not shown). Cells were fixed and labelled with
1141 antibodies against endogenous dynein LIC1 and GFP. **(C)** Line scans (black lines on the
1142 images) were performed and are shown on the right: LIC1 shown in black, GFP-KASH5 in
1143 green. Wide-field imaging; scale bar = 10 µm. **(D)** The samples were scored for dynein
1144 recruitment (see methods; 100 cells per condition, in each of 3 independent repeats). **(E)**
1145 GFP-tagged KASH5ΔK, GFP-KASHΔK EF-hand mutants, or GFP were expressed in HeLaM cells
1146 then fixed and labelled with antibodies to GFP and GM130 then scored for Golgi apparatus
1147 morphology in a blinded fashion (100 cells per condition, in each of 3 independent repeats).
1148 Statistical analysis is given in Table S3.
1149

1150 **Supplementary Figure 1. Effect of IC2 and LIS1 depletion on dynein and dynactin**
1151 **recruitment to KASH5.**
1152 **(A)** Illustration depicting how the meiotic LINC complex connects telomeres inside the
1153 nucleus to cytoplasmic dynein in the cytoplasm. The telomeres (black dots) associate with
1154 SUN1 or SUN2 at the inner nuclear membrane (INM). KASH5 couples to dynein at the outer
1155 nuclear membrane (ONM), dragging the telomeres towards the centrosome (yellow dots) in
1156 leptotene of prophase I, generating the chromosome 'bouquet' in zygotene. This movement
1157 allows pairing of homologous chromosomes (shades of green, blue and red/orange) and the
1158 formation of the synaptonemal complex (black bars). For simplicity, only 6 chromosomes
1159 are depicted. **(B)** A schematic showing the subunits of dynein, dynactin, and a DDA motor-
1160 adaptor complex. **(C)** HeLa cells stably expressing GFP-KASH5 (green) were depleted of IC2
1161 using 20 nM siRNA for 72 hours and then processed for immunofluorescence with
1162 antibodies against LIC1, dynactin p150 and LIS1. Cells were scored in a binary fashion for
1163 recruitment of IC, LIC1 or p150 to KASH5. The mean and standard deviation is shown for
1164 three independent repeats in which 300 cells were scored for each condition per
1165 experiment. **(D-G)** HeLa cells stably expressing inducible GFP-KASH5 were depleted of LIS1
1166 using 20 nM siRNA, induced to express GFP-KASH5 and then fixed and labelled. **(D)** Cells
1167 were scored in a binary fashion to determine if cells showed recruitment IC, LIC1 or p150 to
1168 KASH5. The mean and standard deviation is shown for four independent repeats in which
1169 300 cells were scored for each condition per experiment. Statistical tests were determined
1170 as not being appropriate for the data in B or C, as there is no variation in some control
1171 conditions. Immunofluorescence images showing GFP-KASH5 in green and antibodies
1172 against dynein LIC1 **(E)**, IC **(F)** and dynactin p150 **(G)** in magenta. Images were taken on a
1173 DeltaVision microscope followed by deconvolution. Images are Z-stack projections. Thin
1174 white lines on colour images are site of line scans which are shown on the right. Scale bars
1175 represent 10 µm.
1176
1177 **Supplementary Figure 2. Immunoblot analysis demonstrating depletion of targets by**
1178 **RNAi.**
1179 **(A)** HeLa cells stably expressing inducible GFP-KASH5 were depleted of various dynein
1180 subunits or LIS1 using 20 nM siRNAs against the following targets: Control (Sc), LIC1, LIC2,
1181 LIC1&2, IC2 and LIS1. Representative western blots of cell lysates of knockdown cells are

1182 shown. Blots were probed with antibodies against GFP, p150, IC, LIC1, LIC2, LIS1 and α-
1183 tubulin. Molecular weight markers are shown on the right. Knockdown efficiency was
1184 analysed by quantification of blots using Image Studio software, with correction for protein
1185 loading using the anti-tubulin signal. Experiments were repeated four times alongside
1186 immunofluorescence experiments. Error bars represent standard deviations. **(B)**
1187 Immunoblotting of HeLaM cells depleted with 5 nM each of LIC1 and LIC2 duplexes, or 10
1188 nM control duplexes, for 72 hours. Blots were probed with antibodies to dynein LIC1, LIC2,
1189 IC (IC74) and dynactin p150. Mean efficiency of knockdowns (±S.D.) was analysed as above,
1190 for n=3 independent experiments. **(C)** Quantitation of siRNA efficiency for LICs individually
1191 and together, in HeLaM cells (n=3, ±S.D.), including the data depicted in Fig. 5A.
1192
1193 **Supplementary Figure 3. LICs 1 and 2 act redundantly in endocytic organelle positioning,**
1194 **with helix 1 being essential.**
1195 **(A)** HeLaM cells were depleted of Lamin A/C or LIC 1 and 2 using 5 nM of each siRNA duplex
1196 and stained for organelle markers (EEA1, early endosomes; LAMP1, lysosomes; TfR,
1197 recycling endosomes). **(B)** LIC-depleted cells were transfected with siRNA-resistant LIC1-
1198 mKate or LIC2-GFP and antibody labelled. The boxed region in the LAMP1 image is shown at
1199 two different focal planes. Asterisks mark transfected cells. **(C, D)** LIC depleted cells were
1200 transfected with GFP-LIC1 FL, CT2, CT3 or GFP. Asterisks mark transfected cells. Control
1201 knockdown cells were not transfected. Cells were labelled with anti-EEA1 **(C)** or anti-LAMP1
1202 **(D)**. All images are wide-field. Scale bars = 10 µm. Early endosome and lysosome position
1203 phenotypes were scored as outlined in **(E)**, with ~100 cells per condition, repeated in 3
1204 independent experiments. GFP and GFP-LIC1-CT3 rescue data are significantly different to
1205 control knockdown (P≤0.0001), whereas rescue with GFP-LIC1-FL or GFP-LIC1-CT2 are not
1206 (multinomial logistic regression, see table S4).
1207
1208 **Supplementary Figure 4. LICs act redundantly to recruit dynein and dynactin to RILP-**
1209 **positive late endosomes, and recruitment requires helix 1.**
1210 **(A-D)** Cells were depleted of LICs individually or together for 48 hours using a total of 20 nM
1211 siRNA then transfected with GFP-RILP and fixed 1 day later and labelled for IC **(A)** or
1212 dynactin p150 **(B)**. Control cells (not siRNA treated) were transfected with GFP-RILP.
1213 DeltaVision deconvolved images are shown as z-stack projections. Scale bar = 10 µm. The

1214 percentage of cells with GFP-RILP structures labelled with IC **(C)** or p150 **(D)** was scored (±
1215 S.D.). At least 100 cells were scored in each of three independent experiments. *** =
1216 P<0.001, **** = P<0.0001, one-way ANOVA with Dunnett's post-hoc test. **(E)** HeLaM cells
1217 were co-transfected with HA-RILP and GFP-LIC1 full length, CT2 or CT3. Wide-field images
1218 are shown; scale bar = 10 µm.
1219
1220 **Supplementary Figure 5. Effect of calcium depletion on dynein recruitment to KASH5 and**
1221 **Rab11-FIP3.**
1222 Following transient transfection of HeLa M cells with GFP-KASH5-FL **(A)** or Vero cells with
1223 GFP-Rab11-FIP3 **(B)**, cells were treated with either DMSO vehicle control or 10 µM BAPTA-
1224 AM for 2 hours at 37°C. Cells were fixed and labelled with antibodies to GFP and
1225 endogenous LIC1. Wide-field images, with boxed regions shown as enlargements in **(B)**.
1226 Scale bars represent 10 µm. **(C)** Lysates of HeLaM cells expressing either GFP or GFP-
1227 KASH5ND were used for GFP-trap in the presence or absence of 1 mM EGTA. Beads and
1228 inputs (15% of the GFP-trap samples) were probed for endogenous LIC1 or GFP by
1229 immunoblotting. An un-paired T-test was used to compare levels of LIC1 pulled down with
1230 KASH5 ± EGTA (n=3 independent experiments, P=0.592).
1231
1232
1233 **References**
1234

1235 Addinall, S., P. Mayr, S. Doyle, J. Sheehan, P. Woodman, and V. Allan. 2001. Phosphorylation
1236 by cdc2-cyclinB1 kinase releases cytoplasmic dynein from membranes. *J. Biol. Chem.*
1237 276:15939-15944. doi:10.1074/jbc.M011628200.
1238 Agrawal, R., J.P. Gillies, J.L. Zang, J. Zhang, S.R. Garrott, H. Shibuya, J. Nandakumar, and M.E.
1239 DeSantis. 2022. The KASH5 protein involved in meiotic chromosomal movements is a
1240 novel dynein activating adaptor. *eLife*. 11:e78201. doi:10.7554/eLife.78201.
1241 Apolonia, L., R. Schulz, T. Curk, P. Rocha, C.M. Swanson, T. Schaller, J. Ule, and M.H. Malim.
1242 2015. Promiscuous RNA binding ensures effective encapsidation of APOBEC3
1243 proteins by HIV-1. *PLoS Pathog.* 11:e1004609. doi:10.1371/journal.ppat.1004609.
1244 Baffet, A.D., D.J. Hu, and R.B. Vallee. 2015. Cdk1 activates pre-mitotic nuclear envelope
1245 dynein recruitment and apical nuclear migration in neural stem cells. *Dev. Cell*.
1246 33:703-716. doi:10.1016/j.devcel.2015.04.022.
1247 Baumbach, J., A. Murthy, M.A. McClintock, C.I. Dix, R. Zalyte, H.T. Hoang, and S.L. Bullock.
1248 2017. Lissencephaly-1 is a context-dependent regulator of the human dynein
1249 complex. *eLife*. 6:e21768. doi:10.7554/eLife.21768.

1250 Belyy, V., M.A. Schlager, H. Foster, A.E. Reimer, A.P. Carter, and A. Yildiz. 2016. The
1251 mammalian dynein-dynactin complex is a strong opponent to kinesin in a tug-of-war
1252 competition. *Nat. Cell Biol.* 18:1018-1024. doi:10.1038/ncb3393.
1253 Bentebbal, S.A., B.R. Meqbel, A. Salter, V. Allan, B. Burke, and H.F. Horn. 2021. A human
1254 infertility-associated KASH5 variant promotes mitochondrial localization. *Sci. Rep.*
1255 11:10133. doi:10.1038/s41598-021-89439-2.
1256 Bielli, A., P.-O. Thörnqvist, A. Hendrick, R. Finn, K. Fitzgerald, and M. McCaffrey. 2001. The
1257 small GTPase Rab4A interacts with the central region of cytoplasmic dynein light
1258 intermediate chain-1. *Biochem. Biophys. Res. Comm.* 281:1141-1153.
1259 doi:10.1006/bbrc.2001.4468.
1260 Burke, B. 2018. LINC complexes as regulators of meiosis. *Curr. Opin. Cell Biol.* 52:22-29.
1261 doi:10.1016/j.ceb.2018.01.005.
1262 Canty, J.T., and A. Yildiz. 2020. Activation and regulation of cytoplasmic dynein. *Trends*
1263 *Biochem. Sci.* 45:440-453. doi:10.1016/j.tibs.2020.02.002.
1264 Celestino, R., M.A. Henen, J.B. Gama, C. Carvalho, M. McCabe, D.J. Barbosa, A. Born, P.J.
1265 Nichols, A.X. Carvalho, R. Gassmann, and B. Vogeli. 2019. A transient helix in the
1266 disordered region of dynein light intermediate chain links the motor to structurally
1267 diverse adaptors for cargo transport. *PLoS Biol.* 17:e3000100.
1268 doi:10.1371/journal.pbio.3000100.
1269 Chaaban, S., and A.P. Carter. 2022. Structure of dynein-dynactin on microtubules shows
1270 tandem adaptor binding. *Nature*. 610:212-216. doi:10.1038/s41586-022-05186-y.
1271 Chapman, D.E., B.J.N. Reddy, B. Huy, M.J. Bovyn, S.J.S. Cruz, Z.M. Al-Shammari, H. Han, W.
1272 Wang, D.S. Smith, and S.P. Gross. 2019. Regulation of in vivo dynein force production
1273 by CDK5 and 14-3-3epsilon and KIAA0528. *Nat. Commun.* 10:228.
1274 doi:10.1038/s41467-018-08110-z.
1275 Chi, Y.H., L.I. Cheng, T. Myers, J.M. Ward, E. Williams, Q. Su, L. Faucette, J.Y. Wang, and K.T.
1276 Jeang. 2009. Requirement for Sun1 in the expression of meiotic reproductive genes
1277 and piRNA. *Development*. 136:965-973. doi:10.1242/dev.029868.
1278 Chowdhury, S., S.A. Ketcham, T.A. Schroer, and G.C. Lander. 2015. Structural organization of
1279 the dynein-dynactin complex bound to microtubules. *Nat. Struct. Mol. Biol.* 22:345-
1280 347. doi:doi:10.1038/nsmb.2996.
1281 Christensen, J.R., A.A. Kendrick, J.B. Truong, A. Aguilar-Maldonado, V. Adani, M.
1282 Dzieciatkowska, and S.L. Reck-Peterson. 2021. Cytoplasmic dynein-1 cargo diversity
1283 is mediated by the combinatorial assembly of FTS-Hook-FHIP complexes. *eLife*.
1284 10:e74538. doi:10.7554/eLife.74538.
1285 Cockell, M.M., K. Baumer, and P. Gonczy. 2004. Lis-1 is required for dynein-dependent cell
1286 division processes in C. elegans embryos. *J. Cell Sci.* 117:4571-4582.
1287 doi:10.1242/jcs.01344.
1288 Colucci, A.M., M.C. Campana, M. Bellopede, and C. Bucci. 2005. The Rab-interacting
1289 lysosomal protein, a Rab7 and Rab34 effector, is capable of self-interaction.
1290 *Biochem. Biophys. Res. Commun.* 334:128-133. doi:10.1016/j.bbrc.2005.06.067.
1291 Dekens, M.P.S., F.J. Pelegri, H.-M. Maischein, and C. Nüsslein-Volhard. 2003. The maternal-
1292 effect gene futile cycle is essential for pronuclear congression and mitotic spindle
1293 assembly in the zebrafish zygote. *Development*. 130:3907-3916.
1294 doi:10.1242/dev.00606.

1295 Ding, X., R. Xu, J. Yu, T. Xu, Y. Zhuang, and M. Han. 2007. SUN1 is required for telomere
1296 attachment to nuclear envelope and gametogenesis in mice. *Dev. Cell*. 12:863-872.
1297 doi:10.1016/j.devcel.2007.03.018.
1298 Dix, C., H. Soundararajan, N. Dzhindzhev, F. Begum, B. Suter, H. Ohkura, E. Stephens, and S.
1299 Bullock. 2013. Lissencephaly-1 promotes the recruitment of dynein and dynactin to
1300 transported mRNAs. *J. Cell Biol.* 202:479-494. doi:10.1083/jcb.201211052.
1301 Driskell, O., A. Mironov, V. Allan, and P. Woodman. 2007. Dynein is required for receptor
1302 sorting and the morphogenesis of early endosomes. *Nat. Cell Biol.* 9:113-120.
1303 doi:10.1038/ncb1525.
1304 Dunce, J.M., A.E. Milburn, M. Gurusaran, I. da Cruz, L.T. Sen, R. Benavente, and O.R. Davies.
1305 2018. Structural basis of meiotic telomere attachment to the nuclear envelope by
1306 MAJIN-TERB2-TERB1. *Nat. Commun.* 9:5355. doi:10.1038/s41467-018-07794-7.
1307 Dwivedi, D., A. Kumari, S. Rathi, S.V.S. Mylavarapu, and M. Sharma. 2019. The dynein
1308 adaptor Hook2 plays essential roles in mitotic progression and cytokinesis. *J. Cell*
1309 *Biol.* 218:871-894. doi:10.1083/jcb.201804183.
1310 Dzhindzhev, N.S., S.L. Rogers, R.D. Vale, and H. Ohkura. 2005. Distinct mechanisms govern
1311 the localisation of Drosophila CLIP-190 to unattached kinetochores and microtubule
1312 plus-ends. *J. Cell Sci.* 118:3781-3790. doi:10.1242/jcs.02504.
1313 Elshenawy, M.M., J.T. Canty, L. Oster, L.S. Ferro, Z. Zhou, S.C. Blanchard, and A. Yildiz. 2019.
1314 Cargo adaptors regulate stepping and force generation of mammalian dynein-
1315 dynactin. *Nat. Chem. Biol.* 15:1093-1101. doi:10.1038/s41589-019-0352-0.
1316 Elshenawy, M.M., E. Kusakci, S. Volz, J. Baumbach, S.L. Bullock, and A. Yildiz. 2020. Lis1
1317 activates dynein motility by modulating its pairing with dynactin. *Nat. Cell Biol.*
1318 22:570-578. doi:10.1038/s41556-020-0501-4.
1319 Even, I., S. Reidenbach, T. Schlechter, N. Berns, R. Herold, W. Roth, D. Krunic, V. Riechmann,
1320 and I. Hofmann. 2019. DLIC1, but not DLIC2, is upregulated in colon cancer and this
1321 contributes to proliferative overgrowth and migratory characteristics of cancer cells.
1322 *FEBS J.* 286:803-820. doi:10.1111/febs.14755.
1323 Feng, Q., A.M. Gicking, and W.O. Hancock. 2020. Dynactin p150 promotes processive
1324 motility of DDB complexes by minimizing diffusional behavior of dynein. *Mol. Biol.*
1325 *Cell*. 31:782-792. doi:10.1091/mbc.E19-09-0495.
1326 Fenton, A.R., T.A. Jongens, and E.L.F. Holzbaur. 2021. Mitochondrial adaptor TRAK2
1327 activates and functionally links opposing kinesin and dynein motors. *Nat. Commun.*
1328 12:4578. doi:10.1038/s41467-021-24862-7.
1329 Flores-Rodriguez, N., S. Rogers, D. Kenwright, T. Waigh, P. Woodman, and V. Allan. 2011.
1330 Roles of dynein and dynactin in early endosome dynamics revealed using automated
1331 tracking and global analysis. *PLoS ONE*. 6:e24479.
1332 doi:10.1371/journal.pone.0024479.
1333 Gama, J.B., C. Pereira, P.A. Simoes, R. Celestino, R.M. Reis, D.J. Barbosa, H.R. Pires, C.
1334 Carvalho, J. Amorim, A.X. Carvalho, D.K. Cheerambathur, and R. Gassmann. 2017.
1335 Molecular mechanism of dynein recruitment to kinetochores by the Rod-Zw10-
1336 Zwilch complex and Spindly. *J. Cell Biol.* 216:943-960. doi:10.1083/jcb.201610108.
1337 Gill, S.R., T.A. Schroer, I. Szilak, E.R. Steuer, and M.P. Sheetz. 1991. Dynactin, a conserved,
1338 ubiquitously expressed component of an activator of vesicle motility mediated by
1339 cytoplasmic dynein. *J. Cell Biol.* 115:1639-1650. doi:10.1083/jcb.115.6.1639.

1340 Gillies, J.P., J.M. Reimer, E.P. Karasmanis, I. Lahiri, Z.M. Htet, A.E. Leschziner, and S.L. Reck-
1341 Peterson. 2022. Structural basis for cytoplasmic dynein-1 regulation by Lis1. *eLife*.
1342 11:e71229. doi:10.7554/eLife.71229.
1343 Goncalves, J.C., T.J. Dantas, and R.B. Vallee. 2019. Distinct roles for dynein light
1344 intermediate chains in neurogenesis, migration, and terminal somal translocation. *J.*
1345 *Cell Biol.* 218:808-819. doi:10.1083/jcb.201806112.
1346 Gönczy, P., S. Pichler, M. Kirkham, and A. Hyman. 1999. Cytoplasmic dynein is required for
1347 distinct aspects of MTOC positioning, including centrosome separation, in the one
1348 cell stage *Caenorhabditis elegans* embryo. *J. Cell Biol.* 147:135-150.
1349 doi:10.1083/jcb.147.1.135.
1350 Grabarek, Z. 2006. Structural basis for diversity of the EF-hand calcium-binding proteins. *J.*
1351 *Mol. Biol.* 359:509-525. doi:10.1016/j.jmb.2006.03.066.
1352 Granger, E., G. McNee, V. Allan, and P. Woodman. 2014. The role of the cytoskeleton and
1353 molecular motors in endosomal dynamics. *Semin. Cell Dev. Biol.* 31:20-29.
1354 doi:10.1016/j.semcdb.2014.04.011.
1355 Grotjahn, D.A., S. Chowdhury, Y. Xu, R.J. McKenney, T.A. Schroer, and G.C. Lander. 2018.
1356 Cryo-electron tomography reveals that dynactin recruits a team of dyneins for
1357 processive motility. *Nat. Struct. Mol. Biol.* 25:203-207. doi:10.1038/s41594-018-
1358 0027-7.
1359 Guo, X., G.G. Farias, R. Mattera, and J.S. Bonifacino. 2016. Rab5 and its effector FHF
1360 contribute to neuronal polarity through dynein-dependent retrieval of
1361 somatodendritic proteins from the axon. *Proc. Natl. Acad. Sci. USA*. 113:E5318-5327.
1362 doi:10.1073/pnas.1601844113.
1363 Gurusaran, M., and O.R. Davies. 2021. A molecular mechanism for LINC complex branching
1364 by structurally diverse SUN-KASH 6:6 assemblies. *eLife*. 10:e60175.
1365 doi:10.7554/eLife.60175.
1366 Gutierrez, P.A., B.E. Ackermann, M. Vershinin, and R.J. McKenney. 2017. Differential effects
1367 of the dynein-regulatory factor Lissencephaly-1 on processive dynein-dynactin
1368 motility. *J. Biol. Chem.* 292:12245-12255. doi:10.1074/jbc.M117.790048.
1369 Hao, H., and D.A. Starr. 2019. SUN/KASH interactions facilitate force transmission across the
1370 nuclear envelope. *Nucleus*. 10:73-80. doi:10.1080/19491034.2019.1595313.
1371 Hoogenraad, C., A. Akhmanova, S. Howell, B. Dortland, C. de Zeeuw, R. Willemsen, P. Visser,
1372 F. Grosveld, and N. Galjart. 2001. Mammalian Golgi-associated Bicaudal-D2 functions
1373 in the dynein-dynactin pathway by interacting with these complexes. *EMBO J.*
1374 20:4041-4054. doi:10.1093/emboj/20.15.4041.
1375 Hoogenraad, C., P. Wulf, N. Schiefermeier, T. Stepanova, N. Galjart, J. Small, F. Grosveld, C.
1376 de Zeeuw, and A. Akhmanova. 2003. Bicaudal D induces selective dynein-mediated
1377 microtubule minus end-directed transport. *EMBO J.* 22:6004-6015.
1378 doi:10.1093/emboj/cdg592.
1379 Horgan, C.P., S.R. Hanscom, R.S. Jolly, C.E. Futter, and M.W. McCaffrey. 2010a. Rab11-FIP3
1380 binds dynein light intermediate chain 2 and its overexpression fragments the Golgi
1381 complex. *Biochem. Biophys. Res. Commun.* 394:387-392.
1382 doi:10.1016/j.bbrc.2010.03.028.
1383 Horgan, C.P., S.R. Hanscom, R.S. Jolly, C.E. Futter, and M.W. McCaffrey. 2010b. Rab11-FIP3
1384 links the Rab11 GTPase and cytoplasmic dynein to mediate transport to the
1385 endosomal-recycling compartment. *J. Cell Sci.* 123:181-191. doi:10.1242/jcs.052670.

1386 Horgan, C.P., S.R. Hanscom, and M.W. McCaffrey. 2011. Dynein LIC1 localises to the mitotic
1387 spindle and midbody and LIC2 localises to spindle poles during cell division. *Cell Biol.*
1388 *Int.* doi:10.1042/CBI20100284.
1389 Horn, H., D.I. Kim, G. Wright, E. Wong, C. Stewart, B. Burke, and K. Roux. 2013. A
1390 mammalian KASH domain protein coupling meiotic chromosomes to the
1391 cytoskeleton. *J. Cell Biol.* 202:1023-1039. doi:10.1083/jcb.201304004.
1392 Htet, Z.M., J.P. Gillies, R.W. Baker, A.E. Leschziner, M.E. DeSantis, and S.L. Reck-Peterson.
1393 2020. LIS1 promotes the formation of activated cytoplasmic dynein-1 complexes.
1394 *Nat. Cell Biol.* 22:518-525. doi:10.1038/s41556-020-0506-z.
1395 Hunt, S., A. Townley, C. Danson, P.J. Cullen, and D.J. Stephens. 2013. Microtubule motors
1396 mediate endosomal sorting by maintaining functional domain organization. *J. Cell*
1397 *Sci.* 126:2493-2501. doi:10.1242/jcs.122317.
1398 Jha, R., J. Roostalu, N.I. Cade, M. Trokter, and T. Surrey. 2017. Combinatorial regulation of
1399 the balance between dynein microtubule end accumulation and initiation of directed
1400 motility. *EMBO J*. 36:3387-3404. doi:10.15252/embj.201797077.
1401 Johansson, M., N. Rocha, W. Zwart, I. Jordens, L. Janssen, C. Kuijl, V. Olkkonen, and J.
1402 Neefjes. 2007. Activation of endosomal dynein motors by stepwise assembly of
1403 Rab7-RILP-p150Glued, ORP1L and the receptor bIII spectrin. *J. Cell Biol.* 176:459-471.
1404 doi:10.1083/jcb.200606077.
1405 Jones, L., C. Villemant, T. Starborg, A. Salter, G. Goddard, P. Ruane, P. Woodman, N.
1406 Papalopulu, S. Woolner, and V. Allan. 2014. Dynein light intermediate chains
1407 maintain spindle bipolarity by functioning in centriole cohesion. *J. Cell Biol.* 207:499-
1408 516. doi:10.1083/jcb.201408025.
1409 Jordens, I., M. Fernandez-Borja, M. Marsman, S. Dusseljee, L. Janssen, J. Calafat, H. Janssen,
1410 R. Wubbolts, and J. Neefjes. 2001. The Rab7 effector protein RILP controls lysosomal
1411 transport by inducing the recruitment of dynein-dynactin motors. *Curr. Biol.*
1412 11:1680-1685. doi:10.1016/s0960-9822(01)00531-0.
1413 Karki, S., and E.L.F. Holzbaur. 1995. Affinity chromatography demonstrates a direct binding
1414 between cytoplasmic dynein and the dynactin complex. *J. Biol. Chem.* 270:28806-
1415 28811. doi:10.1074/jbc.270.48.28806.
1416 Kim, H.J., C. Liu, and A.F. Dernburg. 2022. How and why chromosomes interact with the
1417 cytoskeleton during meiosis. *Genes*. 13:901. doi:10.3390/genes13050901.
1418 King, S., C. Brown, K. Maier, N. Quintyne, and T. Schroer. 2003. Analysis of the dynein-
1419 dynactin interaction in vitro and in vivo. *Mol. Biol. Cell*. 14:5089-5097.
1420 doi:10.1091/mbc.e03-01-0025.
1421 Kumari, A., C. Kumar, R. Pergu, M. Kumar, S.P. Mahale, N. Wasnik, and S.V.S. Mylavarapu.
1422 2021a. Phosphorylation and Pin1 binding to the LIC1 subunit selectively regulate
1423 mitotic dynein functions. *J. Cell Biol.* 220:e202005184. doi:10.1083/jcb.202005184.
1424 Kumari, A., C. Kumar, N. Wasnik, and S.V.S. Mylavarapu. 2021b. Dynein light intermediate
1425 chains as pivotal determinants of dynein multifunctionality. *J. Cell Sci.*
1426 134:jcs.254870. doi:10.1242/jcs.254870.
1427 Lam, C., M.A. Vergnolle, L. Thorpe, P. Woodman, and V. Allan. 2010. Functional interplay
1428 between LIS1, NDE1 and NDEL1 in dynein-dependent organelle positioning. *J. Cell*
1429 *Sci.* 123:202-212. doi:10.1242/jcs.059337.
1430 Lau, C.K., F.J. O'Reilly, B. Santhanam, S.E. Lacey, J. Rappsilber, and A.P. Carter. 2021. Cryo-
1431 EM reveals the complex architecture of dynactin's shoulder region and pointed end.
1432 *EMBO J.* 40:e106164. doi:10.15252/embj.2020106164.

1433 Lee, C.Y., H.F. Horn, C.L. Stewart, B. Burke, E. Bolcun-Filas, J.C. Schimenti, M.E. Dresser, and
1434 R.J. Pezza. 2015. Mechanism and regulation of rapid telomere prophase movements
1435 in mouse meiotic chromosomes. *Cell Rep.* 11:551-563.
1436 doi:10.1016/j.celrep.2015.03.045.
1437 Lee, I.G., S.E. Cason, S.S. Alqassim, E.L.F. Holzbaur, and R. Dominguez. 2020. A tunable LIC1-
1438 adaptor interaction modulates dynein activity in a cargo-specific manner. *Nat.*
1439 *Commun.* 11:5695. doi:10.1038/s41467-020-19538-7.
1440 Lee, I.G., M.A. Olenick, M. Boczkowska, C. Franzini-Armstrong, E.L.F. Holzbaur, and R.
1441 Dominguez. 2018. A conserved interaction of the dynein light intermediate chain
1442 with dynein-dynactin effectors necessary for processivity. *Nat. Commun.* 9:986.
1443 doi:10.1038/s41467-018-03412-8.
1444 Lei, K., X. Zhang, X. Ding, X. Guo, M. Chen, B. Zhu, T. Xu, Y. Zhuang, R. Xu, and M. Han. 2009.
1445 SUN1 and SUN2 play critical but partially redundant roles in anchoring nuclei in
1446 skeletal muscle cells in mice. *Proc. Natl. Acad. Sci. USA*. 106:10207-10212.
1447 doi:10.1073/pnas.0812037106.
1448 Lindeman, R.E., and F. Pelegri. 2012. Localized products of futile cycle/ lrmp promote
1449 centrosome-nucleus attachment in the zebrafish zygote. *Curr. Biol.* 22:843-851.
1450 doi:10.1016/j.cub.2012.03.058.
1451 Link, J., M. Leubner, J. Schmitt, E. Gob, R. Benavente, K.T. Jeang, R. Xu, and M. Alsheimer.
1452 2014. Analysis of meiosis in SUN1 deficient mice reveals a distinct role of SUN2 in
1453 mammalian meiotic LINC complex formation and function. *PLoS Genet.*
1454 10:e1004099. doi:10.1371/journal.pgen.1004099.
1455 Mahale, S., M. Kumar, A. Sharma, A. Babu, S. Ranjan, C. Sachidanandan, and S.V.S.
1456 Mylavarapu. 2016a. The light intermediate chain 2 subpopulation of dynein
1457 regulates mitotic spindle orientation. *Sci. Rep.* 6:22. doi:10.1038/s41598-016-0030-3.
1458 Mahale, S.P., A. Sharma, and S.V. Mylavarapu. 2016b. Dynein light intermediate chain 2
1459 facilitates the metaphase to anaphase transition by inactivating the spindle assembly
1460 checkpoint. *PLoS One*. 11:e0159646. doi:10.1371/journal.pone.0159646.
1461 Malone, C., L. Misner, N. Le Bot, M.-C. Tsai, J. Campbell, J. Ahringher, and J. White. 2003.
1462 The *C. elegans* hook protein, ZYG12, mediates the essential attachment between the
1463 centrosome and nucleus. *Cell*. 115:825-836. doi:10.1016/s0092-8674(03)00985-1.
1464 Markus, S.M., M.G. Marzo, and R.J. McKenney. 2020. New insights into the mechanism of
1465 dynein motor regulation by lissencephaly-1. *eLife*. 9:e59737.
1466 doi:10.7554/eLife.59737.
1467 Marzo, M.G., J.M. Griswold, and S.M. Markus. 2020. Pac1/LIS1 stabilizes an uninhibited
1468 conformation of dynein to coordinate its localization and activity. *Nat. Cell Biol.*
1469 22:559-569. doi:10.1038/s41556-020-0492-1.
1470 McKenney, R., H. W, M. Tanenbaum, G. Bhabha, and R.D. Vale. 2014. Activation of
1471 cytoplasmic dynein motility by dynactin-cargo adatper complexes. *Science*. 345:337-
1472 341. doi:10.1126/science.1254198
1473 Minn, I.L., M.M. Rolls, W. Hanna-Rose, and C.J. Malone. 2009. SUN-1 and ZYG-12, mediators
1474 of centrosome–nucleus attachment, are a functional SUN/KASH pair in C. elegans.
1475 *Mol. Biol. Cell*. 20:4586-4595. doi:10.1091/mbc.E08.
1476 Morimoto, A., H. Shibuya, X. Zhu, J. Kim, K.i. Ishiguro, M. Han, and Y. Watanabe. 2012. A
1477 conserved KASH domain protein associates with telomeres, SUN1, and dynactin
1478 during mammalian meiosis. *J. Cell Biol.* 198:165-172. doi:10.1083/jcb.201204085.

1479 Niclas, J., V.J. Allan, and R.D. Vale. 1996. Cell cycle regulation of dynein association with
1480 membranes modulates microtubule-based organelle transport. *J. Cell Biol.* 133:585-
1481 593. doi:10.1083/jcb.133.3.585.
1482 Olenick, M.A., R. Dominguez, and E.L.F. Holzbaur. 2019. Dynein activator Hook1 is required
1483 for trafficking of BDNF-signaling endosomes in neurons. *J. Cell Biol.* 218:220-233.
1484 doi:10.1083/jcb.201805016.
1485 Olenick, M.A., and E.L.F. Holzbaur. 2019. Dynein activators and adaptors at a glance. *J. Cell*
1486 *Sci.* 132: jcs227132. doi:10.1242/jcs.227132.
1487 Palmer, K.J., H. Hughes, and D.J. Stephens. 2009. Specificity of cytoplasmic dynein subunits
1488 in discrete membrane trafficking steps. *Mol. Biol. Cell*. 20:2885-2899.
1489 doi:10.1091/mbc.e08-12-1160.
1490 Pandey, J., and D. Smith. 2011. A Cdk5-dependent switch regulates Lis1/Ndel1/dynein-
1491 driven organelle transport in adult neurons. *J. Neurosci.* 31:17207-17219.
1492 doi:10.1523/JNEUROSCI.4108-11.2011.
1493 Payne, C., V. Rawe, J. Ramalho-Santos, C. Simerly, and G. Schatten. 2003. Preferentially
1494 localized dynein and perinuclear dynactin associate with nuclear pore complex
1495 proteins to mediate genomic union during mammalian fertlization. *J. Cell Sci.*
1496 116:4727-4738. doi:10.1242/jcs.00784.
1497 Peranen, J., M. Rikkonen, M. Hyvonen, and L. Kaariainen. 1996. T7 vectors with modified
1498 T7lac promoter for expression of proteins in Escherichia coli. *Anal. Biochem.*
1499 236:371-373. doi:10.1006/abio.1996.0187.
1500 Pfister, K., E. Fisher, I. GIbbons, T. Hays, E. Holzbaur, J. McIntosh, M. Porter, T. Schroer, K.
1501 Vaughan, G. Witman, S. King, and R. Vallee. 2005. Cytoplasmic dynein nomenclature.
1502 *J. Cell Biol.* 171:411-413. doi:10.1083/jcb.200508078.
1503 Qiu, R., J. Zhang, and X. Xiang. 2019. LIS1 regulates cargo-adapter-mediated activation of
1504 dynein by overcoming its autoinhibition in vivo. *J. Cell Biol.* 218:3630-3646.
1505 doi:10.1083/jcb.201905178.
1506 Quintyne, N., S. Gill, D. Eckley, C. Crego, D. Compton, and T. Schroer. 1999. Dynactin is
1507 required for microtubule anchoring at centrosomes. *J. Cell Biol.* 147:321-334.
1508 doi:10.1083/jcb.147.2.321.
1509 Raaijmakers, J., M. Tannenbaum, and R. Medema. 2013. Systematic dissection of dynein
1510 regulators in mitosis. *J. Cell Biol.* 201:201-215. doi:10.1083/jcb.201208098.
1511 Reck-Peterson, S.L., W.B. Redwine, R.D. Vale, and A.P. Carter. 2018. The cytoplasmic dynein
1512 transport machinery and its many cargoes. *Nat. Rev. Mol. Cell Biol.* 19:382-398.
1513 doi:10.1038/s41580-018-0004-3.
1514 Reddy, B.J., M. Mattson, C.L. Wynne, O. Vadpey, A. Durra, D. Chapman, R.B. Vallee, and S.P.
1515 Gross. 2016. Load-induced enhancement of dynein force production by LIS1-NudE in
1516 vivo and in vitro. *Nat. Commun.* 7:12259. doi:10.1038/ncomms12259.
1517 Redwine, W.B., M.E. DeSantis, I. Hollyer, Z.M. Htet, P.T. Tran, S.K. Swanson, L. Florens, M.P.
1518 Washburn, and S.L. Reck-Peterson. 2017. The human cytoplasmic dynein
1519 interactome reveals novel activators of motility. *eLife*. 6:e28257.
1520 doi:10.7554/eLife.28257.
1521 Reiner, O., R. Carrozzo, Y. Shen, M. Wehnert, F. Faustinella, W. Dobyns, T. Caskey, and D.
1522 Ledbetter. 1993. Isolation of a Miller-Dieker lissencephaly gene containing a G
1523 protein b-subunit-like repeat. *Nature*. 364:717-721. doi:10.1038/364717a0.
1524 Reinsch, S., and E. Karsenti. 1997. Movement of nuclei along microtubules in *Xenopus* egg
1525 extracts. *Curr. Biol.* 7:211-214. doi:10.1016/s0960-9822(97)70092-7.

1526 Robinson, J., E. Wojcik, M. Sanders, M. McGrail, and T.S. Hays. 1999. Cytoplasmic dynein is
1527 required for the nuclear attachment and migration of centrosomes duing mitosis in
1528 *Drosophila. J. Cell Biol.* 146:597-608. doi:10.1083/jcb.146.3.597.
1529 Rog, O., and A. Dernburg. 2015. Direct visualization reveals kinetics of meiotic chromosome
1530 synapsis. *Cell Rep.* 10:1639-1645. doi:10.1016/j.celrep.2015.02.032.
1531 Rubin, T., N. Macaisne, and J.R. Huynh. 2020. Mixing and matching chromosomes during
1532 female meiosis. *Cells*. 9:696. doi:10.3390/cells9030696.
1533 Sato, A., B. Isaac, C.M. Phillips, R. Rillo, P.M. Carlton, D.J. Wynne, R.A. Kasad, and A.F.
1534 Dernburg. 2009. Cytoskeletal forces span the nuclear envelope to coordinate meiotic
1535 chromosome pairing and synapsis. *Cell*. 139:907-919. doi:10.1016/j.cell.2009.10.039.
1536 Scherer, J., J. Yi, and R. Vallee. 2014. PKA-dependent dynein switching from lysosomes to
1537 adenovirus: a novel form of host-virus competition. *J. Cell Biol.* 205:163-177.
1538 doi:10.1083/jcb.201307116.
1539 Schlager, M.A., H. Hoang, L. Urnavicius, S. Bullock, and A.P. Carter. 2014a. In vitro
1540 reconstitution of a highly processive recombinant human dynein complex. *EMBO J.*
1541 33:1855-1868. doi: 10.15252/embj.201488792
1542 Schlager, M.A., A. Serra-Marques, I. Grigoriev, L.F. Gumy, M. Esteves da Silva, P.S. Wulf, A.
1543 Akhmanova, and C.C. Hoogenraad. 2014b. Bicaudal d family adaptor proteins control
1544 the velocity of Dynein-based movements. *Cell Rep.* 8:1248-1256.
1545 doi:10.1016/j.celrep.2014.07.052.
1546 Schmitt, J., R. Benavente, D. Hodzic, C. Hoog, C.L. Stewart, and M. Alsheimer. 2007.
1547 Transmembrane protein Sun2 is involved in tethering mammalian meiotic telomeres
1548 to the nuclear envelope. *Proc. Natl. Acad. Sci. USA*. 104:7426-7431.
1549 doi:10.1073/pnas.0609198104.
1550 Schmoranzer, J., J.P. Fawcett, M. Segura, S. Tan, R.B. Vallee, T. Pawson, and G.G. Gundersen.
1551 2009. Par3 and dynein associate to regulate local microtubule dynamics and
1552 centrosome orientation during migration. *Curr. Biol.* 19:1065-1074.
1553 doi:10.1016/j.cub.2009.05.065.
1554 Schroeder, C., J. Olstrem, N. Hertz, and R. Vale. 2014. A Ras-like domain in the light
1555 intermediate chain bridges the dynein motor to a cargo-binding region. *eLife*.
1556 3:e03351-03322. doi:10.7554/eLife.03351.
1557 Schroeder, C.M., and R.D. Vale. 2016. Assembly and activation of dynein–dynactin by the
1558 cargo adaptor protein Hook3. *J. Cell Biol.* 214:309-318. doi:10.1083/jcb.201308009.
1559 Schroer, T.A., and M.P. Sheetz. 1991. Two activators of microtubule-based vesicle transport.
1560 *J. Cell Biol.* 115:1309-1318. doi:10.1083/jcb.115.5.1309.
1561 Sharma, A., S. Dagar, and S.V.S. Mylavarapu. 2020. Transgelin-2 and phosphoregulation of
1562 the LIC2 subunit of dynein govern mitotic spindle orientation. *J. Cell Sci.*
1563 133:jcs239673. doi:10.1242/jcs.239673.
1564 Shibuya, H., K. Ishiguro, and Y. Watanabe. 2014. The TRF1-binding protein TERB1 promotes
1565 chromosome movement and telomere rigidity in meiosis. *Nat. Cell Biol.* 16:145-156.
1566 doi:10.1038/ncb2896.
1567 Siller, K.H., M. Serr, R. Steward, T.S. Hays, and C.Q. Doe. 2005. Live imaging of Drosophila
1568 brain neuroblasts reveals a role for Lis1/dynactin in spindle assembly and mitotic
1569 checkpoint control. *Mol. Biol. Cell*. 16:5127-5140. doi:10.1091/mbc.e05-04-0338.
1570 Sitaram, P., M. Anderson, J. Jodoin, E. Lee, and L. Lee. 2012. Regulation of dynein
1571 localization and centrosome positioning by Lis-1 and asunder during Drosophila
1572 spermatogenesis. *Development*. 39:2945-2954. doi:10.1242/dev.077511.

1573 Sivaram, M.V., T.L. Wadzinski, S.D. Redick, T. Manna, and S.J. Doxsey. 2009. Dynein light
1574 intermediate chain 1 is required for progress through the spindle assembly
1575 checkpoint. *EMBO J.* 28:902-914. doi:10.1038/emboj.2009.38.
1576 Sladewski, T.E., N. Billington, M.Y. Ali, C.S. Bookwalter, H. Lu, E.B. Krementsova, T.A.
1577 Schroer, and K.M. Trybus. 2018. Recruitment of two dyneins to an mRNA-dependent
1578 Bicaudal D transport complex. *eLife*. 7:e36306. doi:10.7554/eLife.36306.
1579 Spindler, M.C., J. Redolfi, F. Helmprobst, P. Kollmannsberger, C. Stigloher, and R. Benavente.
1580 2019. Electron tomography of mouse LINC complexes at meiotic telomere
1581 attachment sites with and without microtubules. *Commun. Biol.* 2:376.
1582 doi:10.1038/s42003-019-0621-1.
1583 Splinter, D., D. Razafsky, M.A. Schlager, A. Serra-Marques, I. Grigoriev, J. Demmers, N.
1584 Keijzer, K. Jiang, I. Poser, A. Hyman, C.C. Hoogenraad, S. King, and A. Akhmanova.
1585 2012. BICD2, dynactin and LIS1 cooperate in regulating dynein recruitment to
1586 cellular structures. *Mol. Biol. Cell*. 23:4226-4241. doi:10.1091/mbc.E12-03-0210.
1587 Srikanth, S., K.D. Kim, Y. Gao, J.S. Woo, S. Ghosh, G. Calmettes, A. Paz, J. Abramson, M.
1588 Jiang, and Y. Gwack. 2016. A large Rab GTPase encoded by CRACR2A is a component
1589 of subsynaptic vesicles that transmit T cell activation signals. *Sci. Signal.* 9:ra31.
1590 doi:10.1126/scisignal.aac9171.
1591 Starr, D.A., and M. Han. 2002. Role of ANC-1 in tethering nuclei to the actin cytoskeleton.
1592 *Science*. 298:406-409. doi:10.1126/science.1075119.
1593 Tan, S., J. Scherer, and R. Vallee. 2011. Recruitment of dynein to late endosomes and
1594 lysosomes through light intermediate chains. *Mol. Biol. Cell*. 22:467-477.
1595 doi:10.1091/mbc.E10-02-0129.
1596 Torisawa, T., M. Ichikawa, A. Furuta, K. Saito, K. Oiwa, H. Kojima, Y.Y. Toyoshima, and K.a.y.
1597 Furuta. 2014. Autoinhibition and cooperative activation mechanisms of cytoplasmic
1598 dynein. *Nat. Cell Biol.* 16:1118-1124. doi:10.1038/ncb3048.
1599 Tsai, J.W., Y. Chen, A.R. Kriegstein, and R.B. Vallee. 2005. LIS1 RNA interference blocks
1600 neural stem cell division, morphogenesis, and motility at multiple stages. *J. Cell Biol.*
1601 170:935-945. doi:10.1083/jcb.200505166.
1602 Tynan, S.H., M.A. Gee, and R.B. Vallee. 2000a. Distinct but overlapping sites within the
1603 cytoplasmic dynein heavy chain for dimerization and for intermediate chain and light
1604 intermediate chain binding. *J. Biol. Chem.* 275:32769-32774.
1605 doi:10.1074/jbc.M001537200.
1606 Tynan, S.H., A. Purohit, S.J. Doxsey, and R.B. Vallee. 2000b. Light intermediate chain 1
1607 defines a functional subfraction of cytoplasmic dynein which binds to pericentrin. *J.*
1608 *Biol. Chem.* 275:32763-32768. doi:10.1074/jbc.M001536200.
1609 Urnavicius, L., C.K. Lau, M.M. Elshenawy, E. Morales-Rios, C. Motz, A. Yildiz, and A.P. Carter.
1610 2018. Cryo-EM shows how dynactin recruits two dyneins for faster movement.
1611 *Nature*. 554:202-206. doi:10.1038/nature25462.
1612 Urnavicius, L., K. Zhang, A.G. Diamant, C. Motz, M.A. Schlager, M. Yu, N.A. Patel, C.V.
1613 Robinson, and A.P. Carter. 2015. The structure of the dynactin complex and its
1614 interaction with dynein. *Science*. 347:2630-2630. doi:10.1126/science.aaa2630.
1615 Vaughan, K.T., and R.B. Vallee. 1995. Cytoplasmic dynein binds dynactin through a direct
1616 interaction between the intermediate chains and p150Glued. *J. Cell Biol.* 131:1507-
1617 1516. doi:10.1083/jcb.131.6.1507.

1618 Villari, G., C. Enrico Bena, M. Del Giudice, N. Gioelli, C. Sandri, C. Camillo, A. Fiorio Pla, C.
1619 Bosia, and G. Serini. 2020. Distinct retrograde microtubule motor sets drive early and
1620 late endosome transport. *EMBO J*. 39:e103661. doi:10.15252/embj.2019103661.
1621 Wang, S., S.A. Ketcham, A. Schon, B. Goodman, Y. Wang, J. Yates, 3rd, E. Freire, T.A. Schroer,
1622 and Y. Zheng. 2013. Nudel/NudE and Lis1 promote dynein and dynactin interaction
1623 in the context of spindle morphogenesis. *Mol. Biol. Cell*. 24:3522-3533.
1624 doi:10.1091/mbc.E13-05-0283.
1625 Wang, Y., W. Huynh, T.D. Skokan, W. Lu, A. Weiss, and R.D. Vale. 2019. CRACR2a is a
1626 calcium-activated dynein adaptor protein that regulates endocytic traffic. *J. Cell Biol.*
1627 218:1619-1633. doi:10.1083/jcb.201806097.
1628 Wilson, G.M., A.B. Fielding, G.C. Simon, X. Yu, P.D. Andrews, R.S. Hames, A.M. Frey, A.A.
1629 Peden, G.W. Gould, and R. Prekeris. 2005. The FIP3-Rab11 protein complex regulates
1630 recycling endosome targeting to the cleavage furrow during late cytokinesis. *Mol.*
1631 *Biol. Cell*. 16:849-860. doi:10.1091/mbc.e04-10-0927.
1632 Wozniak, M., B. Bola, K. Brownhill, Y.-C. Yang, V. Levakova, and V. Allan. 2009. Role of
1633 kinesin-1 and cytoplasmic dynein in endoplasmic reticulum movement in VERO cells.
1634 . *J. Cell Sci.* 122:1979-1989. doi:10.1242/jcs.041962.
1635 Wynne, D., O. Rog, P. Carlton, and A.F. Dernburg. 2012. Dynein-dependent processive
1636 chromsome motions promote homologous pairing in *C. elegans* meiosis. *J. Cell Biol.*
1637 196:47-64. doi:10.1083/jcb.201106022.
1638 Yi, J., K. Ori-McKenney, R. McKenny, M. Vershinin, S. Gross, and R. Vallee. 2011. High-
1639 resolution imaging reveals indirect coordination of opposite motors and a role for
1640 LIS1 in high-load axonal transport. *J. Cell Biol.* 195:193-201.
1641 doi:10.1083/jcb.201104076.
1642 Zhang, K., H.E. Foster, A. Rondelet, S.E. Lacey, N. Bahi-Buisson, A.W. Bird, and A.P. Carter.
1643 2017. Cryo-EM reveals how human cytoplasmic dynein Is auto-inhibited and
1644 activated. *Cell*. 169:1303-1314 e1318. doi:10.1016/j.cell.2017.05.025.
1645 Zufferey, R., D. Nagy, R.J. Mandel, L. Naldini, and D. Trono. 1997. Multiply attenuated
1646 lentiviral vector achieves efficient gene delivery in vivo. *Nat. Biotechnol.* 15:871-875.
1647 doi:10.1038/nbt0997-871.
1648

Garner et al. Figure 1

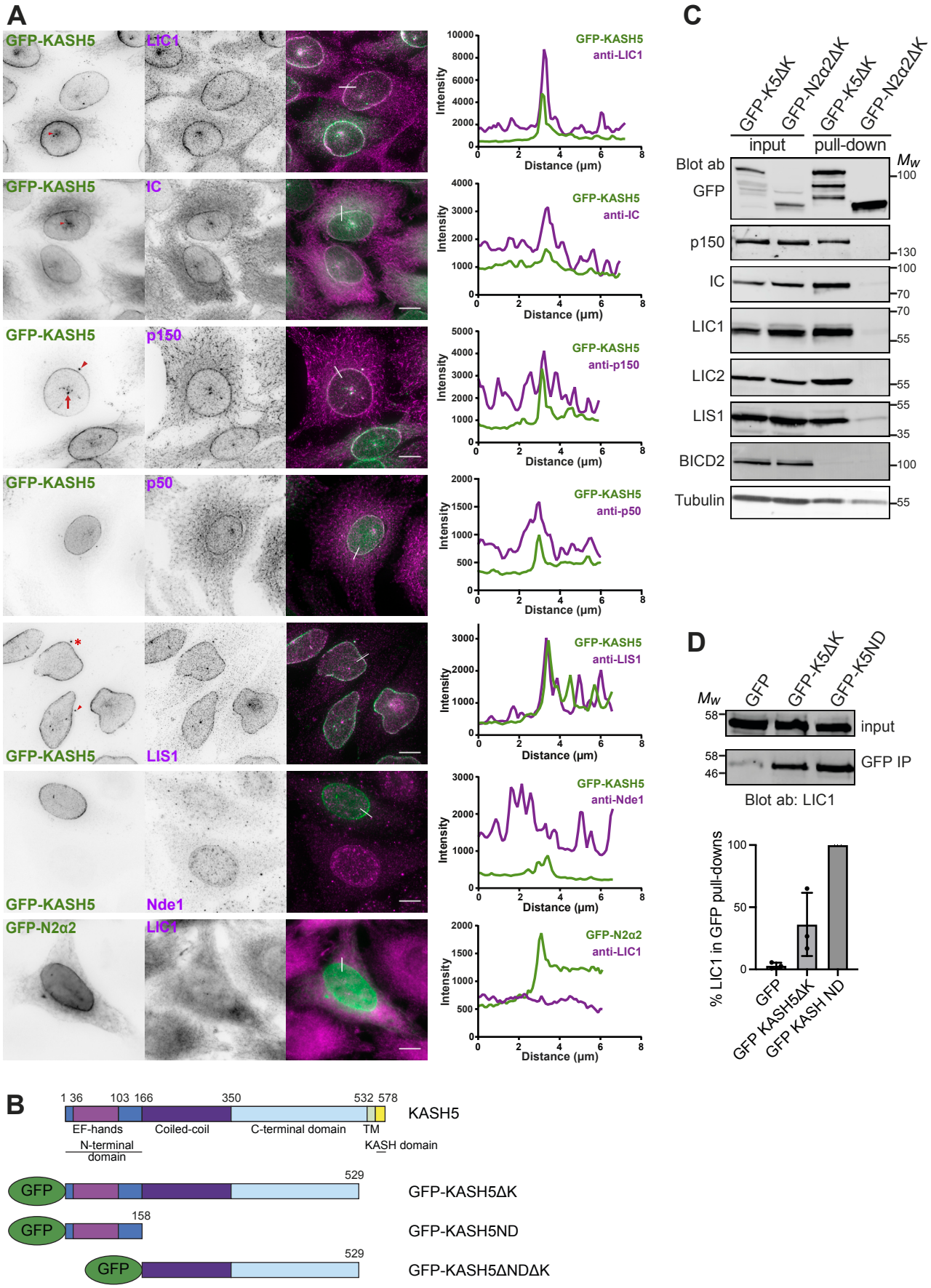

Garner et al. Figure 2

A IC2 siRNA

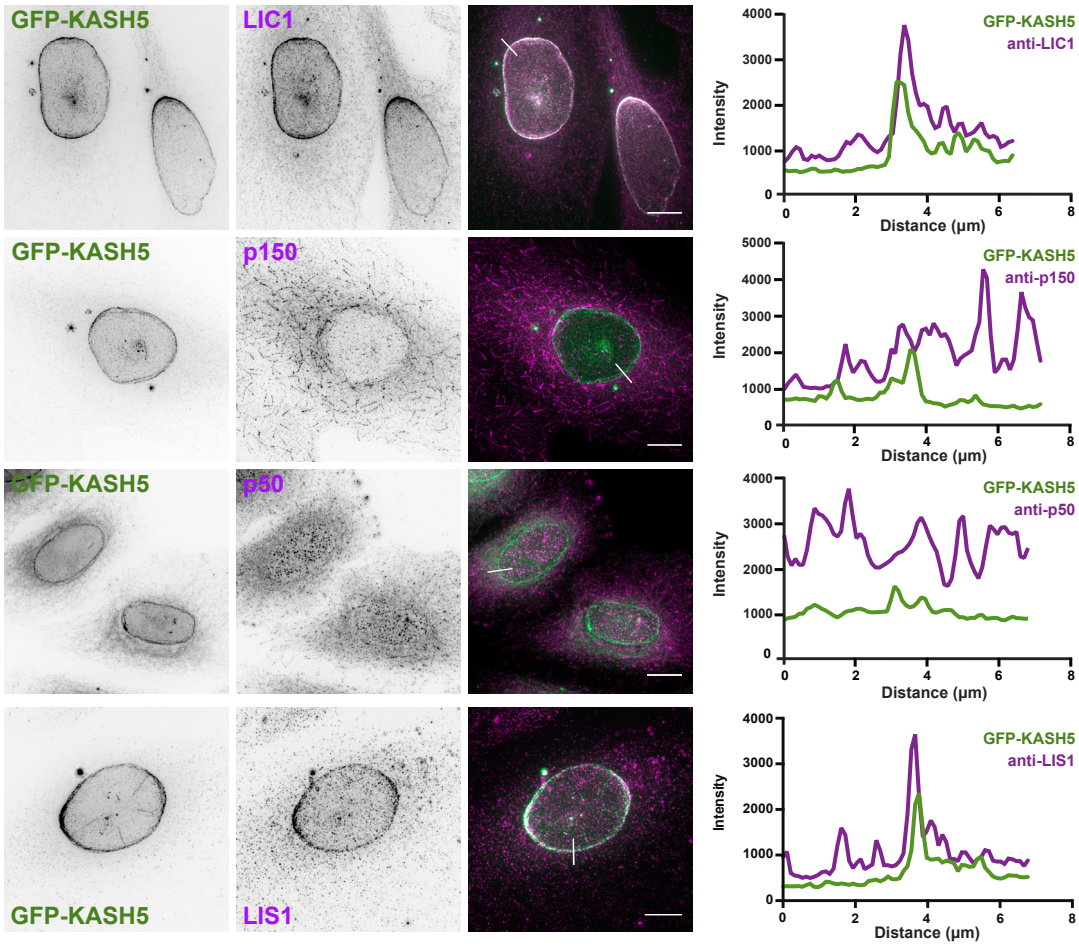

B RFP-p150-CC1 expression

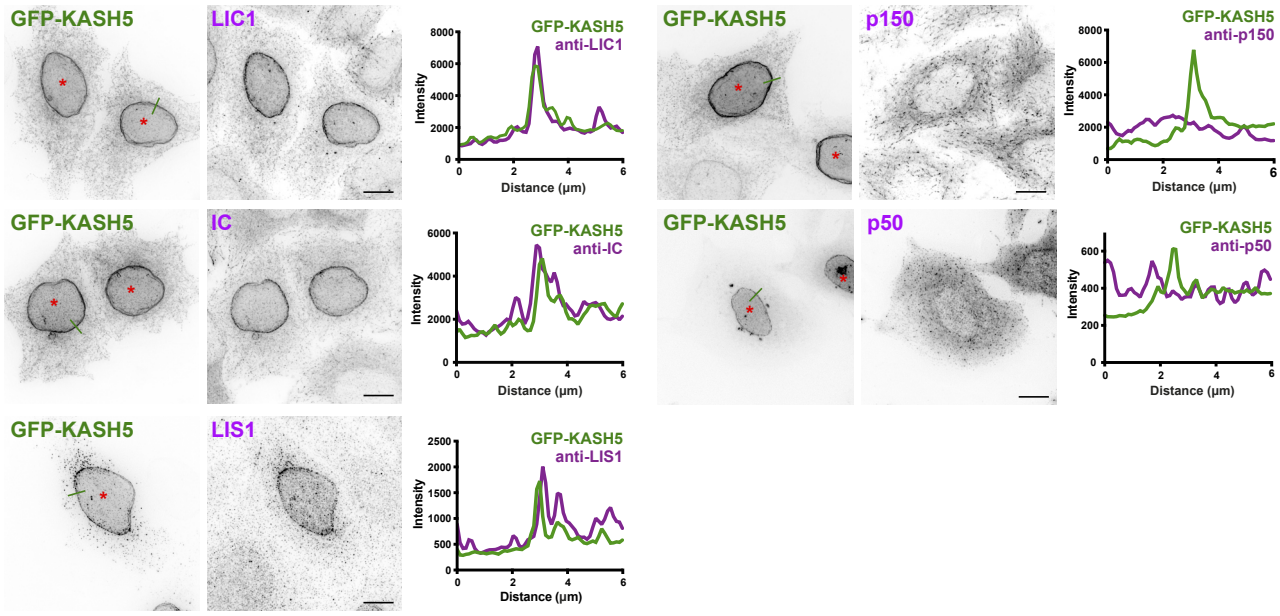

Garner et al. Figure 3

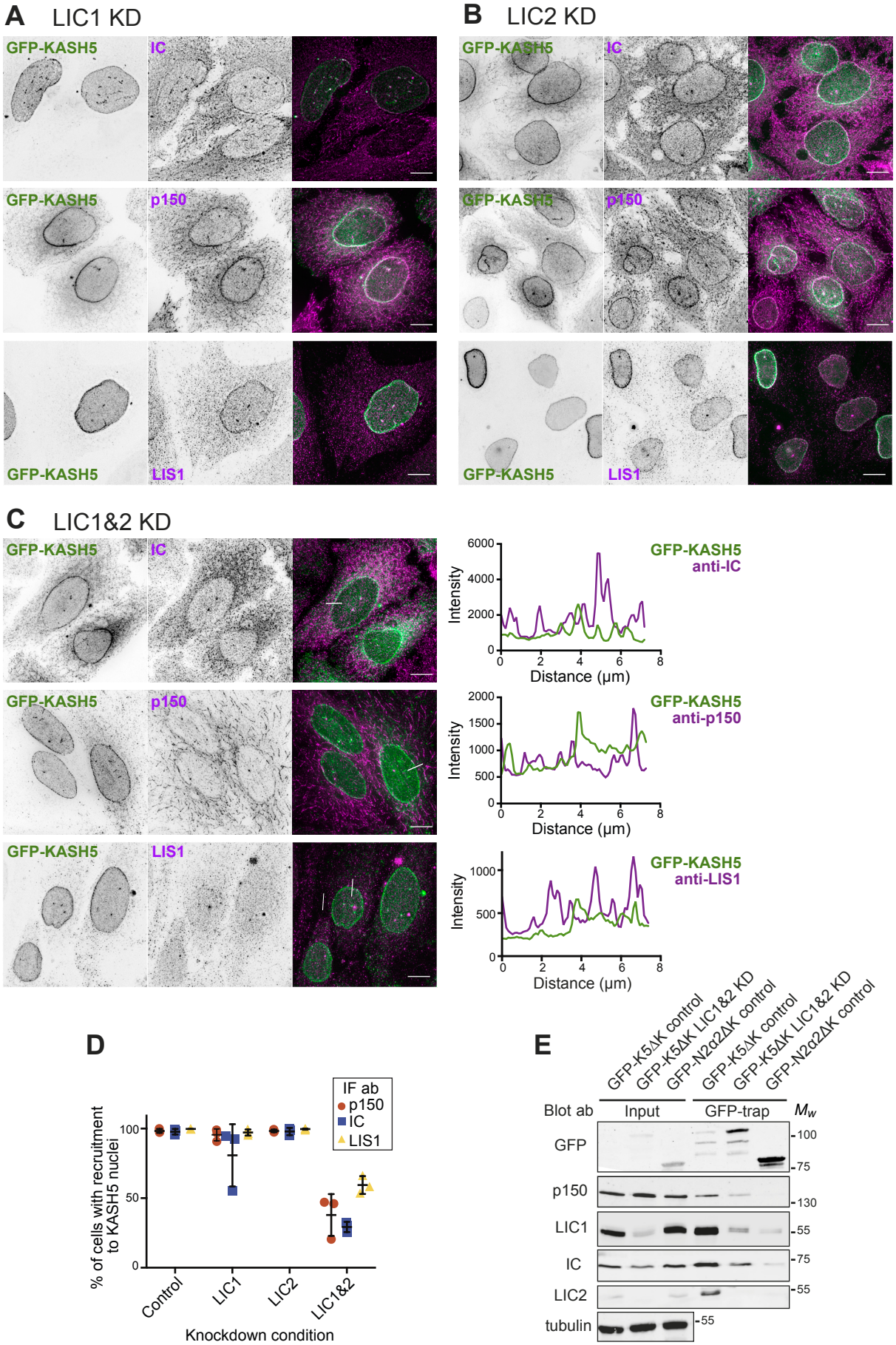

Figure 4, Garner et al.

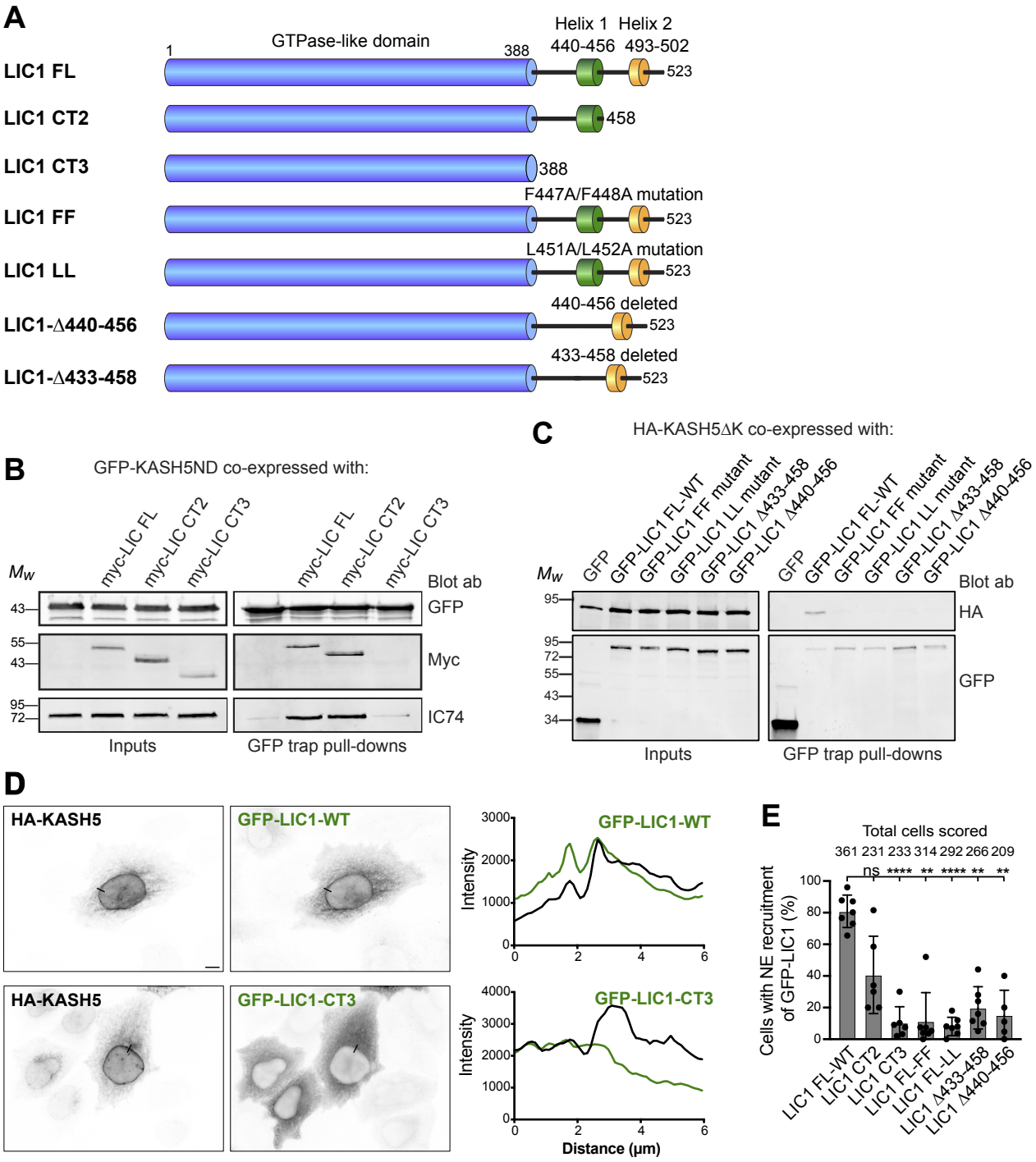

Figure 5, Garner et al.

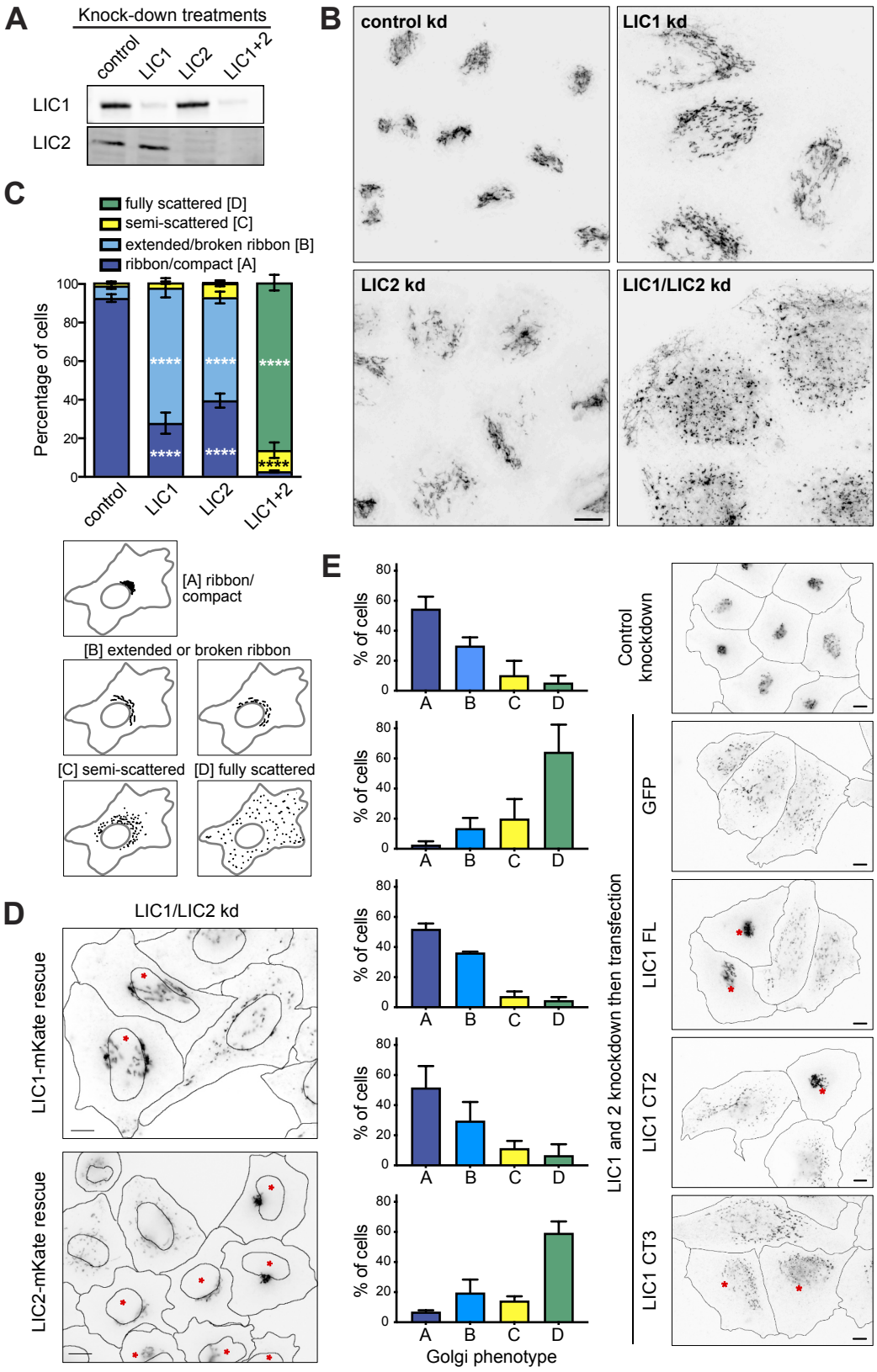

Figure 6, Garner et al.

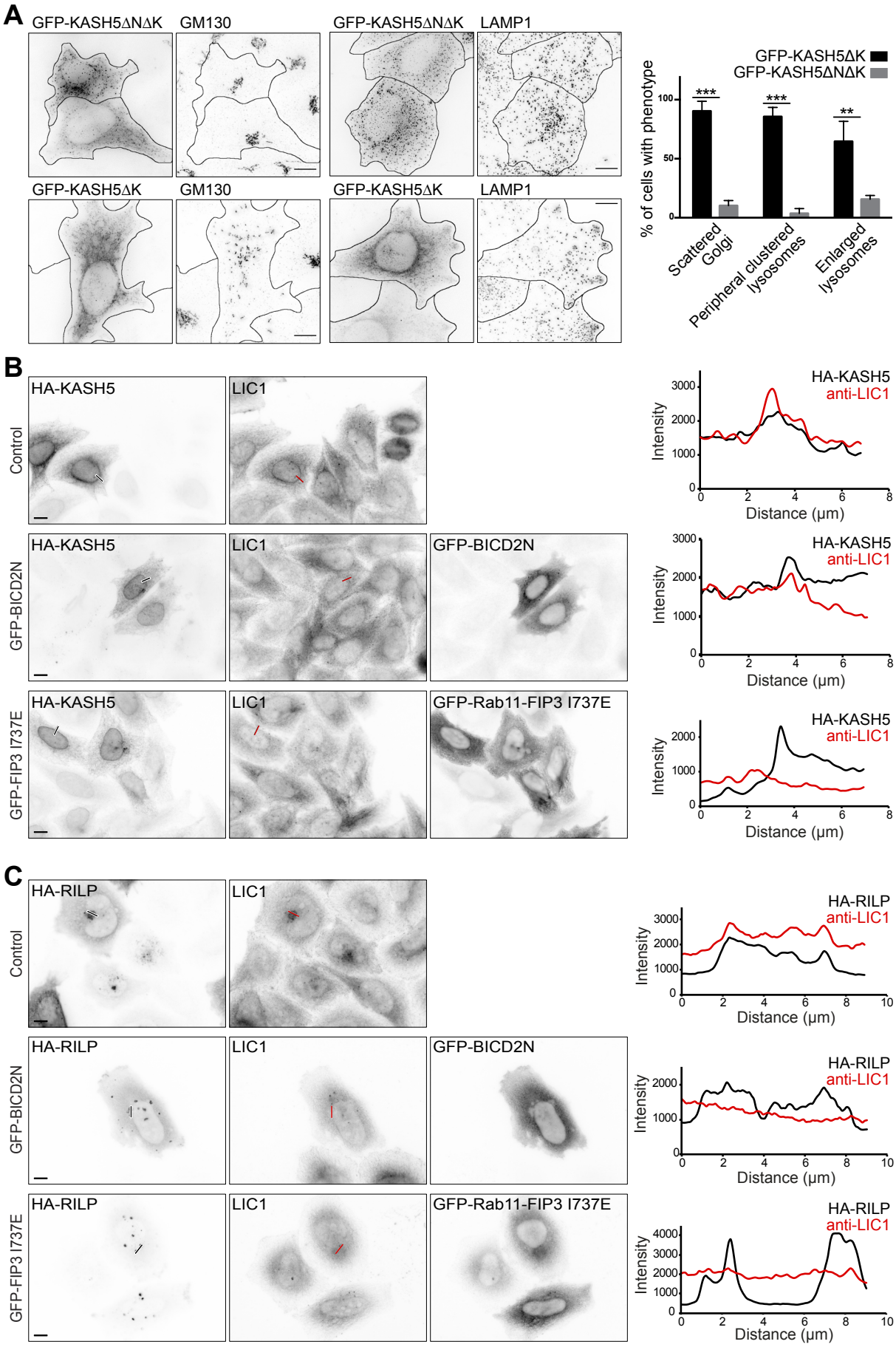

Garner et al. Figure 7

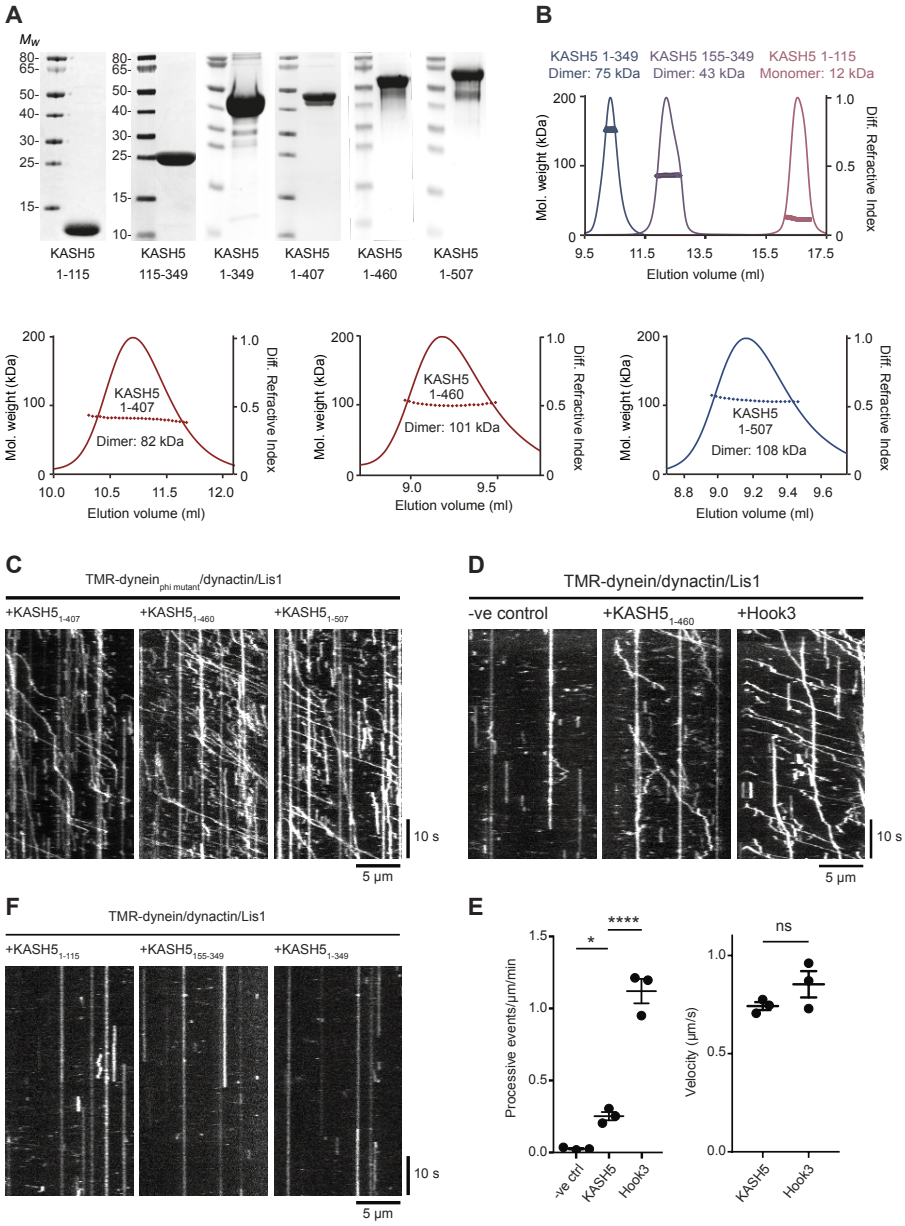
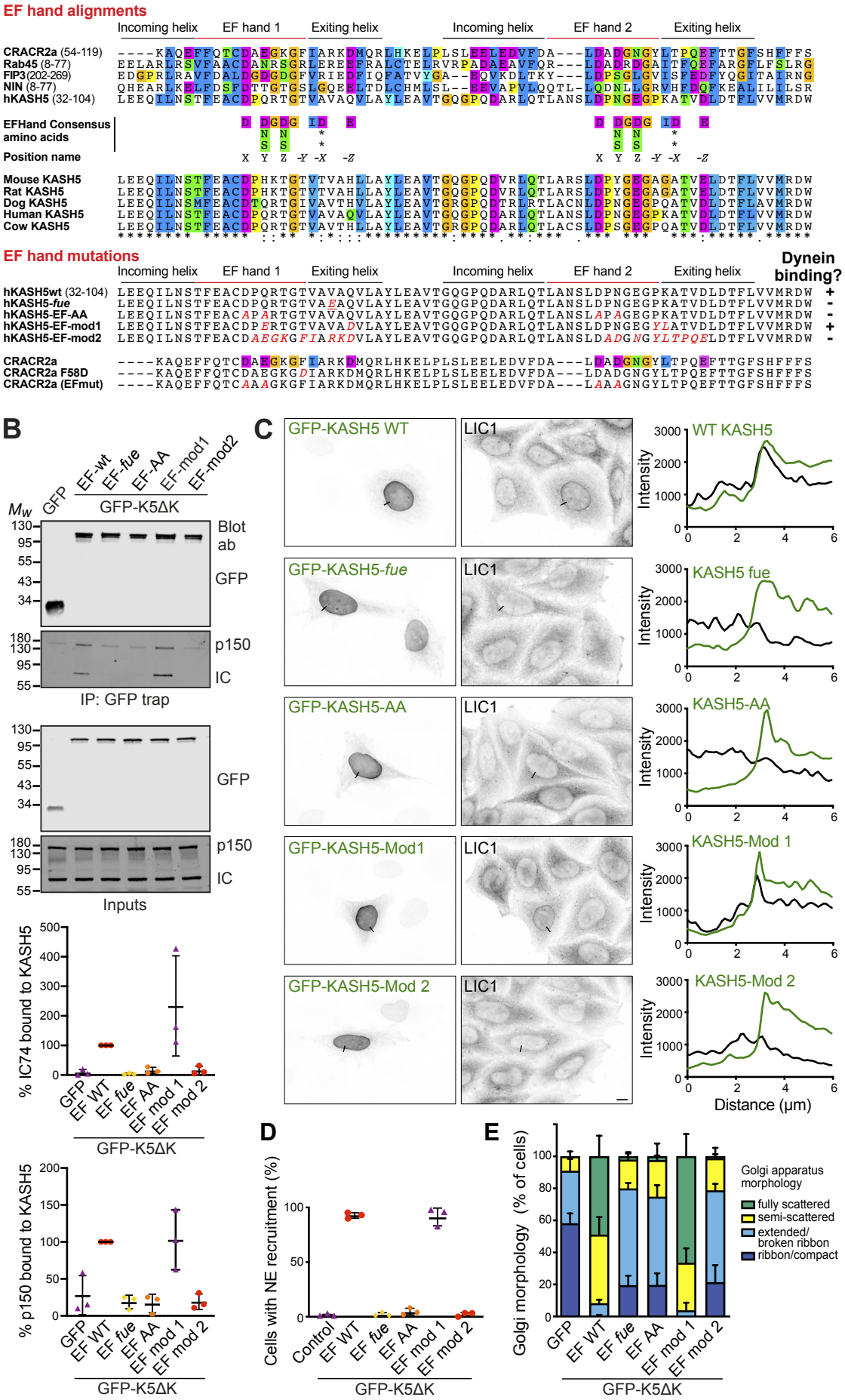
Figure 8, Garner et al.